Chapter 3 Characterisation of *nol9*^{sa1022} mutants

3.1 Introduction

The Zebrafish Mutation Project (ZMP) aims to create a disruptive mutation in every protein-coding gene in the zebrafish genome and to study the phenotypic consequences of such alleles (Kettleborough et al., 2013). During the phenotypic analysis of offspring from incrosses of F2 *nol9*$^{sa1022/+}$, *nol9*$^{sa1022/sa1022}$ (abbreviated as *nol9*^{sa1022}) mutation was found to be associated with a pancreas phenotype (Figure 1-2). The pancreas of *nol9*^{sa1022} larvae was not visible at 5 days post fertilisation (d.p.f.). The ZMP founder fish carry on average seven nonsense mutations, four essential splice and 111 non-synonymous mutations in their exomes that are induced by ENU mutagenesis (Kettleborough et al., 2013). In order to reduce the number of background mutations, I outcrossed the F2 *nol9*$^{sa1022/+}$ adults to SAT wild-type zebrafish.

The *nucleolar protein 9* (*nol9*) gene has three Zv9 Ensembl transcripts: nol9-001, nol9-201 and nol9-002 (Figure 3-1 A). The nol9-001 and nol9-201 are each comprised of 2897 and 2506 bases, respectively, and each have 12 exons encoding a protein of 713 amino acids whilst the nol9-002 is a smaller transcript of 845 bases encoding a protein of 175 amino acids (Figure 3-1 A, B). The NOL9 proteins of human (ENSP00000366934) and mouse (ENSMUSP00000081133) and Nol9 protein in zebrafish (ENSDARP00000123267) are conserved especially in two domains known as *Molybdopterin guanine dinucleotide synthesis protein B* (*MobB*) and *Pre-mRNA cleavage complex II protein* (*Clp1*) (Figure 3-1 B). The zebrafish Nol9 protein has 34% and 30% identical amino acids compared to human and mouse NOL9, respectively. The *nol9*^{sa1022} mutant fish have a C to A mutation in exon 2 converting amino acid 195 from a Tyrosine into a stop codon (Figure 3-1 A, B).

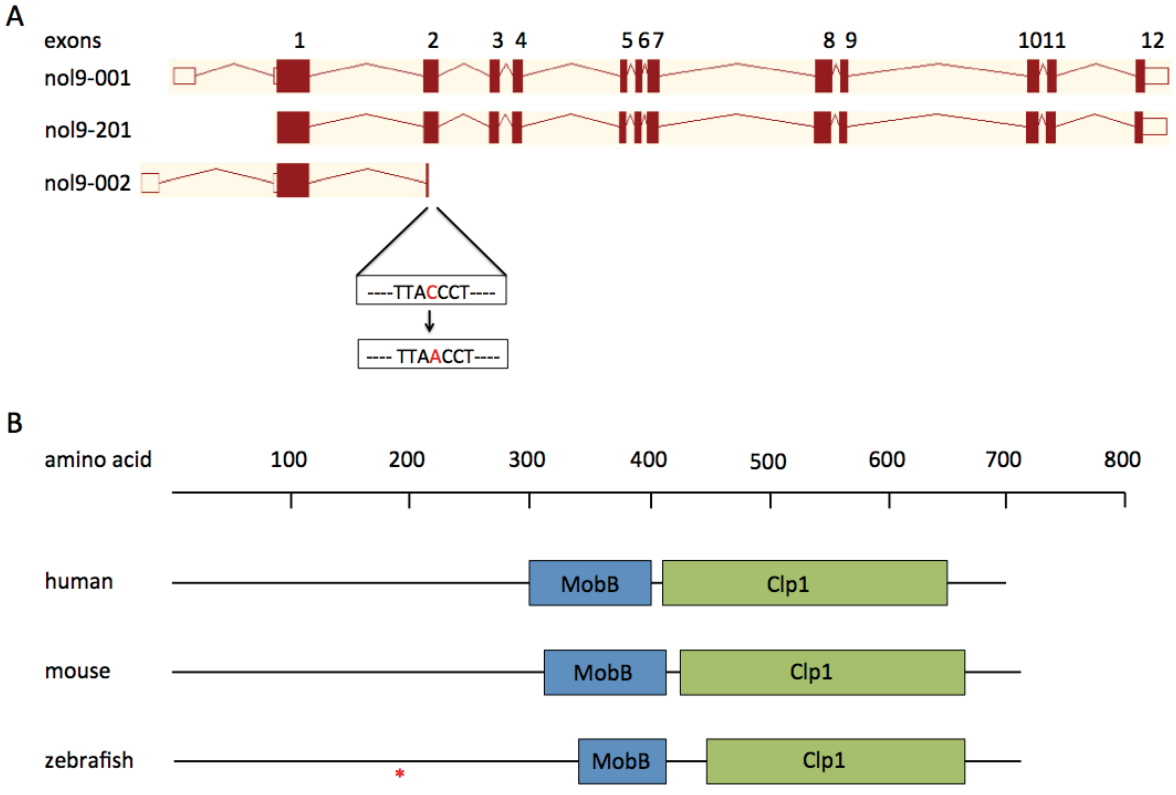

Figure 3-1 Diagram of *nol9* gene and Nol9 protein. (A) The zebrafish *nol9* gene has three Ensembl transcripts nol9-001, nol9-201 and nol9-002. The *nol9*^{sa1022} is a nonsense mutation in exon 2 of transcripts nol9-001 and nol9-201 converting the codon TAC (Tyrosine) into TAA (stop codon). The diagrams were taken from Ensembl. Exons are shown as boxes and introns are shown as lines. (B) The human, mouse and zebrafish Nol9 proteins are conserved. Boxes show the protein domains and * indicates the location of the *nol9*^{sa1022} mutation.

The human NOL9 protein is a polynucleotide 5'-kinase involved in ribosome biogenesis (Heindl and Martinez, 2010). It is a non-ribosomal protein that is required for the efficient generation of the large ribosomal subunit rRNAs, 5.8S and 28S and for the synthesis of the 60S ribosomal subunit (Heindl and Martinez, 2010). As mentioned in Chapter 1, the role of ribosome biogenesis in zebrafish pancreas development has been recognised in recent years. To increase our understanding of this subject, I first aimed to provide further evidence that the *nol9* mutation was causative of the observed pancreas phenotype by phenotyping and genotyping offspring of *nol9*$^{sa1022/+}$ adult, and by recapitulating the pancreas phenotype by morpholino knockdown of *nol9*. Secondly, given that other ribosome biogenesis mutants, including *nil per os* (*npo*) (Mayer and Fishman, 2003), *digestive expansion factor* (*def*) (Chen et al., 2005), *titania* (*tti*) (Boglev et al., 2013) and *nucleolar protein with MIF4G domain 1* (*nom1*) (Qin et al., 2014) also showed defects in the development of the liver and intestine, I aimed to determine whether these organs also showed morphological abnormalities in *nol9*^{sa1022} mutants. Thirdly, I aimed to identify the stage at which the development of the digestive organs is affected by using endodermal markers and developmental markers specific to the pancreas, liver and intestine. Fourthly, I aimed to examine the formation and differentiation of endocrine cells and the formation of secondary islets in *nol9*^{sa1022} mutants. To understand the mechanism of the hypoplastic pancreas phenotype, I studied the cell cycle in *nol9*^{sa1022} mutants, cell proliferation and death of the exocrine pancreas in *nol9*^{sa1022} mutants. As anaemia and craniofacial dysmorphology are common features of ribosomopathies and the zebrafish mutants *npo, def, tti* and *nom1* all exhibit abnormal jaws, I also examined the jaw morphology and erythrocyte development of *nol9*^{sa1022} mutants. The expression pattern of *nol9* during development was then investigated as the expression of *nol9* in the affected organs could help explain the tissue specific defects observed in *nol9*^{sa1022} mutants. Lastly, the functions of Nol9 in rRNA processing and ribosome biogenesis were studied using Northern blotting and polysome fractionation to determine whether Nol9 function is conserved in zebrafish.

3.2 Results

3.2.1 Gross morphology of *nol9*^{sa1022} mutants

The *nol9*^{sa1022} mutants appeared normal up to 4 days post fertilisation (d.p.f.) but at 5 d.p.f. they could be distinguished from wild-type siblings under a dissecting microscope (Figure 3-2). The *nol9*^{sa1022} larvae had fewer folds in their intestine, they had a smaller liver and pancreas and the swim bladders failed to inflate in the majority of larvae. They had no other obvious morphological defects. Thirty 5 d.p.f. phenotypic mutants and thirty wild-type siblings were further grown, by day 10, all the phenotypic *nol9*^{sa1022} mutants had died. These data suggest that *nol9* is involved in the development of digestive organs and that defective development of digestive organs likely underlies the early lethality in *nol9*^{sa1022} mutants.

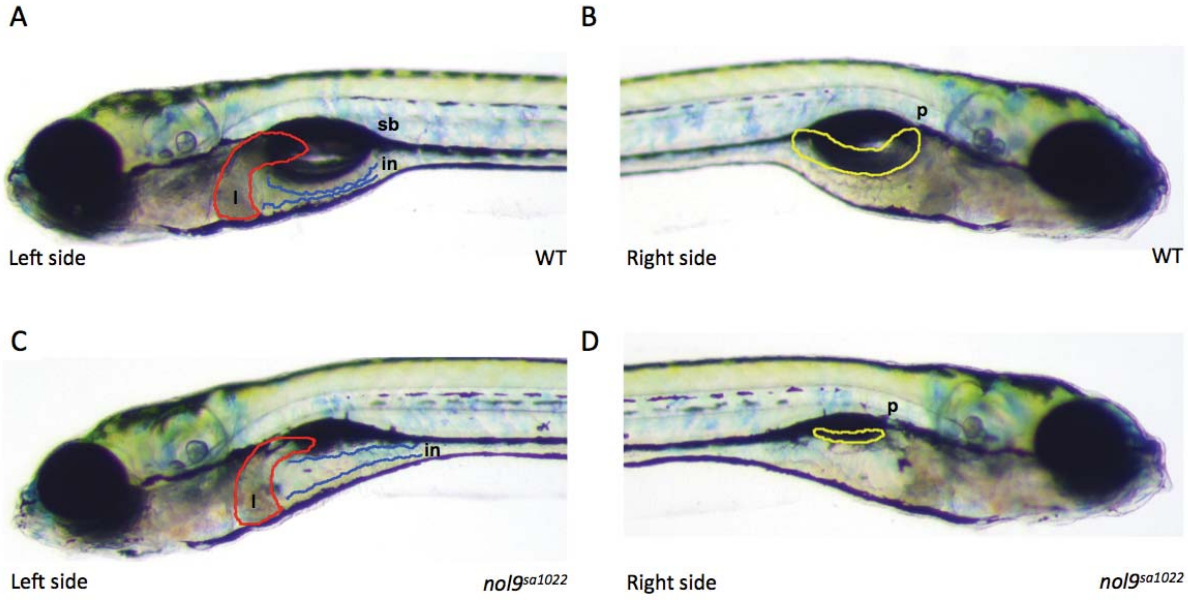

Figure 3-2 The digestive organs of *nol9*^{sa1022} mutants are underdeveloped. (A-D) Bright-field images of 5 d.p.f. wild-type and mutant larvae. (A,C) Left side view of wild-type (A) and *nol9*^{sa1022} larvae (C) showing that *nol9*^{sa1022} mutants have fewer intestinal folds (in; blue), a smaller liver (l; red) and generally uninflated swim bladder (sb) compared to wild-type siblings. (B,D) Right side view of wild-type (B) and *nol9*^{sa1022} larvae (D) showing that *nol9*^{sa1022} mutants have a smaller pancreas (p; yellow) compared to wild-type siblings. (WT) wild-type; (l) liver; (in) intestine; (sb) swim bladder; (p) pancreas.

3.2.2 The *nol9*^{sa1022} mutants have smaller exocrine pancreas

The pancreas of *nol9*^{sa1022} mutants appeared smaller than wild-type siblings under the dissecting microscope. In order to confirm this phenotype and to facilitate the study of pancreas development in *nol9*^{sa1022} mutants, the F2 *nol9*$^{sa1022/+}$ were outcrossed to the transgenic line *Tg(ins:mCherry)*^{jh2}*;Tg(ptf1a:EGFP)*^{jh1} (Pisharath et al., 2007) that expresses mCherry in the pancreatic islet and EGFP in the exocrine pancreas. At 5 d.p.f., the *ptf1a*-positive area of *nol9*^{sa1022} larvae appeared considerably smaller than that of wild-type siblings although the *insulin*-positive area appeared similar in size and shape in *nol9*^{sa1022} and wild-type larvae (Figure 3-3 A, B, Section 2.3.4). The mean volume of *ptf1a*-expressing region of *nol9*^{sa1022} mutants (n=8) is statistically significantly smaller than that of wild-type siblings (n=15), 0.0005 mm^3 and 0.00209 mm^3 respectively (Student's *t*-test, $p = 5.05 \times 10^{-11}$) (Figure 3-3 C, Section 2.3.4). These results demonstrate that the development of the exocrine pancreas is impaired in *nol9*^{sa1022} mutants.

To determine whether the *nol9*^{sa1022} mutation is causative of the small exocrine pancreas phenotype, incrosses of *Tg(ins:mCherry)*^{jh2}*;Tg(ptf1a:EGFP)*^{jh1}*;nol9*$^{sa1022/+}$ were phenotyped at 5 d.p.f based on the size of the *ptf1a*-expressing region and subsequently genotyped (Section 2.1.2). All larvae with a smaller area of *ptf1a*-positive cells were *nol9*$^{sa1022/sa1022}$ (n=36), whereas larvae with normal area of *ptf1a*-positive cells were either *nol9*$^{sa1022/+}$ (n=95) or *nol9*$^{+/+}$ (n=34) (Figure 3-3 D, E). This data indicates that the exocrine pancreas phenotype follows a Mendelian pattern of recessive inheritance and that the *nol9* mutation is linked to the small exocrine pancreas phenotype.

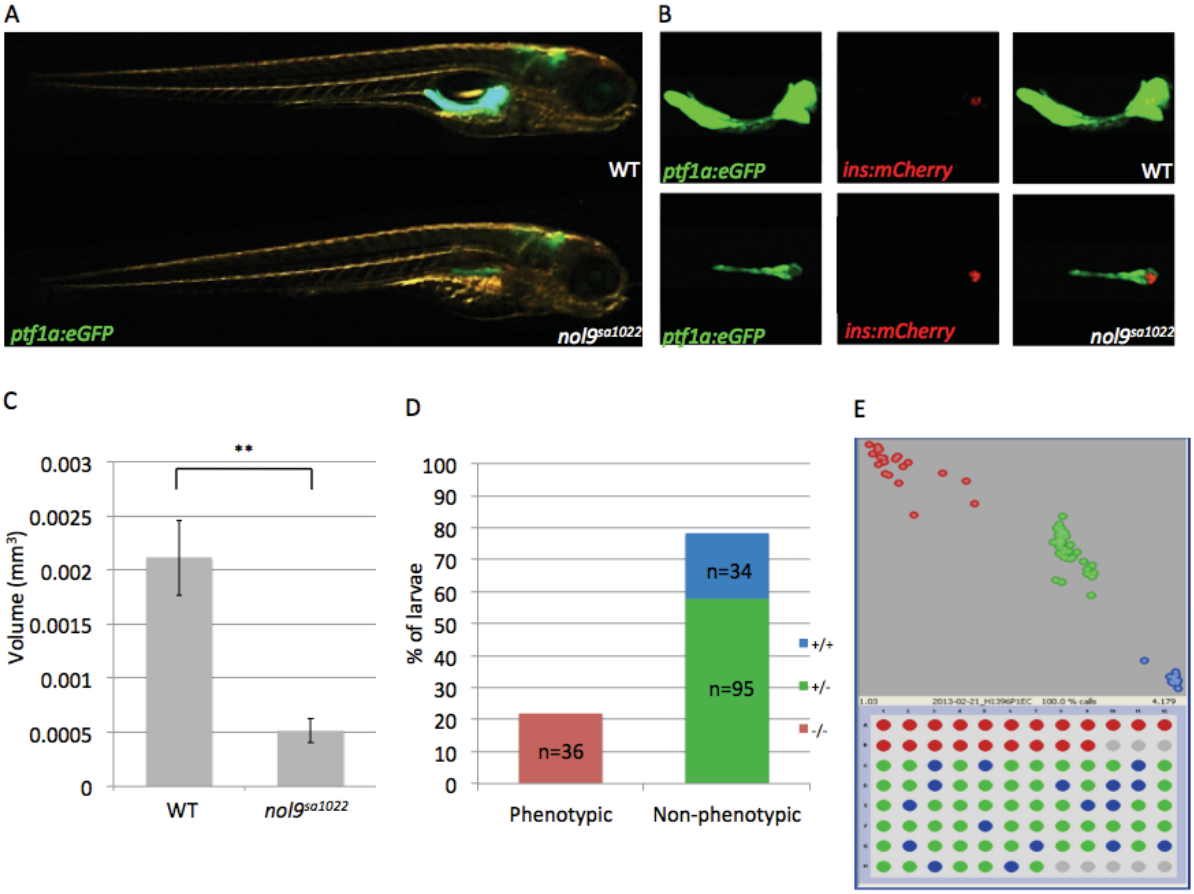

Figure 3-3 The *nol9*^{sa1022} mutation is causative of the exocrine pancreas phenotype. (A) Right side view of 5 d.p.f. *Tg(ins:mCherry)*^{jh2}*;Tg(ptf1a:EGFP)*^{jh1} larvae demonstrating that mutants appear to have a smaller *ptf1a*-positive area compared to wild-type siblings. (B) Confocal images of 5 d.p.f. *Tg(ins:mCherry)*^{jh2}*;Tg(ptf1a:EGFP)*^{jh1} larvae showing that mutants have a smaller *ptf1a*-positive area but normal *ins*-positive area compared to wild-type siblings. (C) The volume of *ptf1a*-expressing region of *nol9*^{sa1022} mutants (n=8) is significantly smaller than wild-type siblings (n=15). Data is represented as the mean ± SD, Student's *t*-test **p<0.01. (D) Graph showing the percentage of phenotypic and non-phenotypic larvae that are homozygous mutant (-/-, red), heterozygous (+/-, green) or homozygous wild-type (+/+, blue) for *nol9*^{sa1022} mutation. (E) Representative image of KASPar genotyping. Phenotypic larvae are in the first two rows and non-phenotypic larvae are in the remaining six rows. The genotype of homozygous mutant, heterozygous and homozygous WT larvae are shown as red, green and blue dots respectively. (WT) wild-type.

3.2.3 Knockdown of *nol9* results in smaller exocrine pancreas

To confirm that the *nol9* mutation is causative of the exocrine pancreas phenotype, *nol9* was knocked down using antisense morpholino oligonucleotide. An ATG morpholino was designed against the translation start site of *nol9* (Section 2.4.1). Wild-type *Tg(ins:mCherry)^{jh2};Tg(ptf1a:EGFP)^{jh1}* embryos were injected with either 4ng *nol9* ATG MO or 4ng standard control morpholino (std MO) (Eisen and Smith, 2008) and treated with phenothiourea (PTU) to inhibit pigmentation and aid in visualising pancreas development. At 4 d.p.f., the *nol9* ATG MO-injected larvae appeared morphologically normal compared to std MO-injected larvae although they sometimes displayed pericardial oedema (Figure 3-4 A). This is consistent with *nol9^{sa1022}* mutants also not displaying any obvious morphological defects at 4 d.p.f. The area of *ptf1a*-positive region appeared smaller in ATG MO-injected larvae compared to std MO-injected larvae whereas the *insulin*-positive signal appeared similar in both ATG MO and std MO-injected zebrafish (Figure 3-4 B, C). Three independent morpholino experiments were carried out and in total, 130 and 169 embryos were injected with std MO and *nol9* MO respectively (Figure 3-4 D). There was a statistically significant difference in the percentage of *nol9* ATG MO-injected, 56.28% and std MO-injected larvae, 5.75% that had a smaller pancreas relative to that of uninjected larvae (Student's *t*-test, p = 0.00359). Likewise, the percentage of larvae that had similar pancreatic size to uninjected larvae was statistically significantly different between *nol9* ATG MO-injected (29.52%) and std MO-injected groups (89.34%) according to the Student's *t*-test (p = 0.00683). There was no statistically significant difference in the percentage of severely delayed larvae in *nol9* ATG MO (14.2%) and std MO-injected (4.44%) zebrafish. This data suggests that knockdown of *nol9* results in smaller exocrine pancreas. To further support this, the pancreatic volume of uninjected, std MO-injected and ATG MO-injected larvae was measured from two independent experiments (Figure 3-4 E, Section 2.3.4). The mean volume of *ptf1a*-expressing region of 4 d.p.f. uninjected (n=20, 0.000609 mm^3) and std MO-injected (n=19, 0.000577 mm^3) larvae was not statistically significantly different from each other (Student's *t*-test, p = 0.555). However, the mean volume of *ptf1a*-expressing region of ATG MO-injected larvae (n=25), 0.000388 mm^3 was significantly smaller than that of uninjected and std MO-injected larvae, with a Student's *t*-test *p*-value of 0.00004 and 0.0000494 respectively. Altogether these results demonstrate that morpholino knockdown of *nol9* recapitulates the *nol9^{sa1022}* phenotype and substantiates the hypothesis that deficiency of *nol9* results in a small exocrine pancreas.

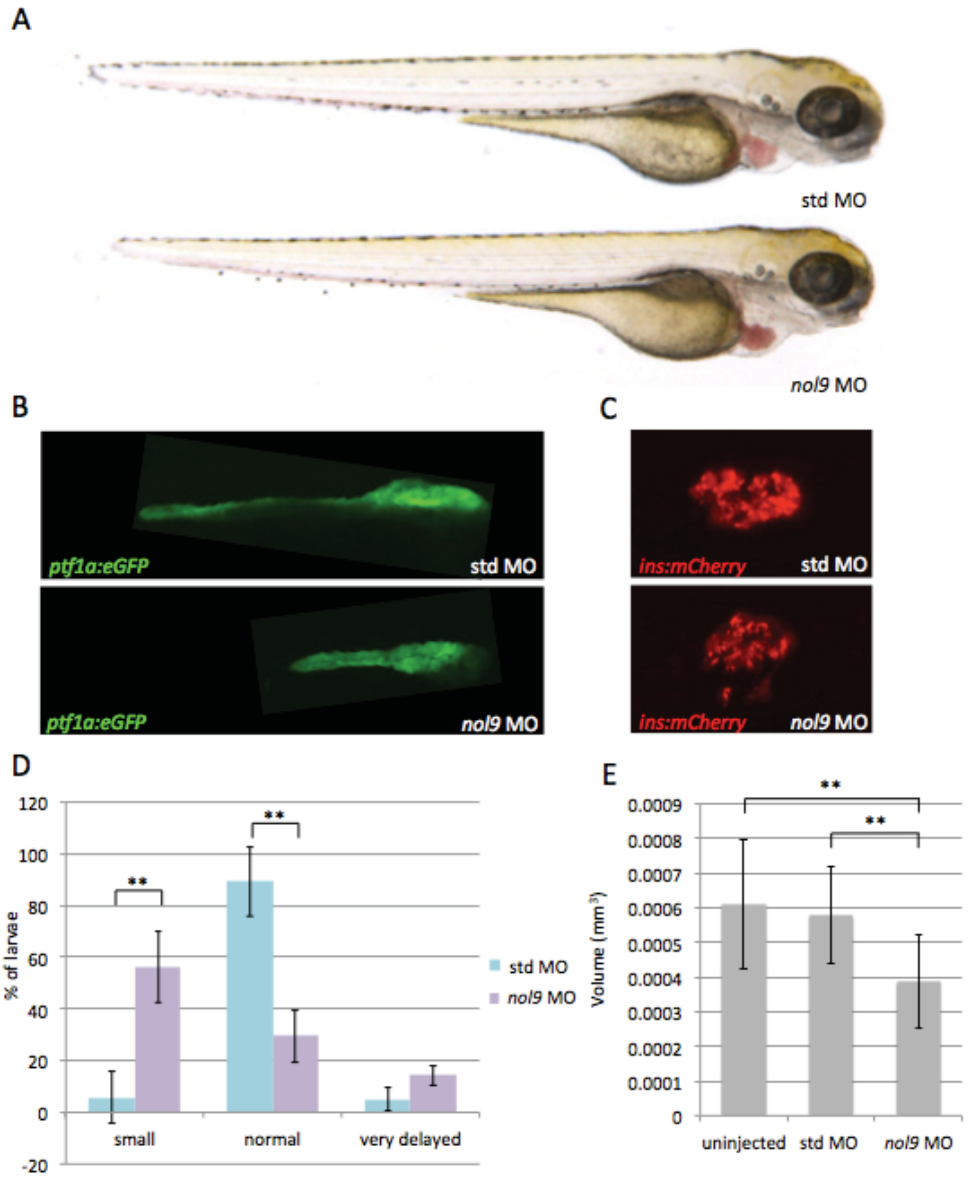

Figure 3-4 Knockdown of *nol9* results in small exocrine pancreas. (A) Right side view of 4 d.p.f. PTU-treated *Tg(ins:mCherry)*^{jh2}*;Tg(ptf1a:EGFP)*^{jh1} fish. The *nol9* ATG MO-injected fish appear morphologically normal compared to std MO-injected fish. (B-C) Representative maximum intensity projection images of a z series of confocal sections through morphants showing that *nol9* MO-injected larvae have a smaller *ptf1a*-positive area (B) compared to std MO-injected larvae whereas the *insulin*-positive signals (C) appear similar in both morphants. (D) Graph showing the percentage of *nol9* MO-injected (n=169) and std MO-injected (n=130) fish from three independent experiments with smaller or normal pancreatic size compared to uninjected larvae and the percentage of larvae that are very delayed. Data is represented as the mean ± SD, Student's *t*-test **p<0.01. (E) Graph showing the volume of *ptf1a*-expressing region of uninjected (n=20), std MO-injected (n=19) and *nol9* MO-injected (n=25) larvae from two independent experiments. Data is represented as the mean ± SD, Student's *t*-test **p<0.01. (std MO) standard control morpholino; (*nol9* MO) *nol9* translation blocking morpholino.

3.2.4 Early development of digestive organs is normal in *nol9*^{sa1022} mutants

The development of zebrafish pancreas consists of different stages including endoderm induction and patterning, cell differentiation of endodermal precursors into specialised pancreatic cells and morphogenesis of the pancreas (Gnugge et al., 2004). To determine the developmental stage at which the pancreas development is impaired in *nol9*^{sa1022} mutants, I first studied the endoderm formation in *nol9*^{sa1022} mutants. This was carried out by examining the expression of the genes *foxa1* (Odenthal and Nusslein-Volhard, 1998) and *gata6* (Wallace et al., 2001), which are expressed in the endodermal lineage during early development of digestive organs. Offspring from an incross of *nol9*$^{sa1022/+}$ carriers were first subjected to whole mount *in situ hybridisation* (ISH) using probes against *foxa1* and *gata6* at 1 d.p.f. and 2 d.p.f. and subsequently genotyped for the *nol9*^{sa1022} mutation (Figure 3-5, Sections 2.1.2 and 2.3.2). At 1 d.p.f., all offspring (n=31) from an incross of *nol9*$^{sa1022/+}$ expressed *foxa1* in the midline and in the pharyngeal endoderm. Six out of these 31 embryos were *nol9*^{sa1022} mutants (Figure 3-5 A). Similarly, all the 1 d.p.f. embryos subjected to *gata6* ISH (n=17) expressed *gata6* in the midline including four that were *nol9*^{sa1022} mutants (Figure 3-5 B). These results indicate that the endodermal layer had formed an endodermal rod in *nol9*^{sa1022} mutants. At 2 d.p.f., all 31 offspring from an incross of *nol9*$^{sa1022/+}$ showed normal expression patterns of *foxa1* including 11 that were *nol9*^{sa1022} mutants (Figure 3-5 C). In addition, all the 2 d.p.f. offspring examined showed similar expression patterns of *gata6* and 15 out of these 56 embryos were *nol9*^{sa1022} mutants (Figure 3-5 D). These results reveal that the formation of the pancreas and liver primordia and gut looping proceed normally in *nol9*^{sa1022} mutants. Overall, the expressions of *foxa1* and *gata6* in *nol9*^{sa1022} mutants demonstrate that the development of digestive organs is normal in *nol9*^{sa1022} mutants before 2 d.p.f., indicating that *nol9* is not involved in the early morphogenesis of the endoderm-derived organs.

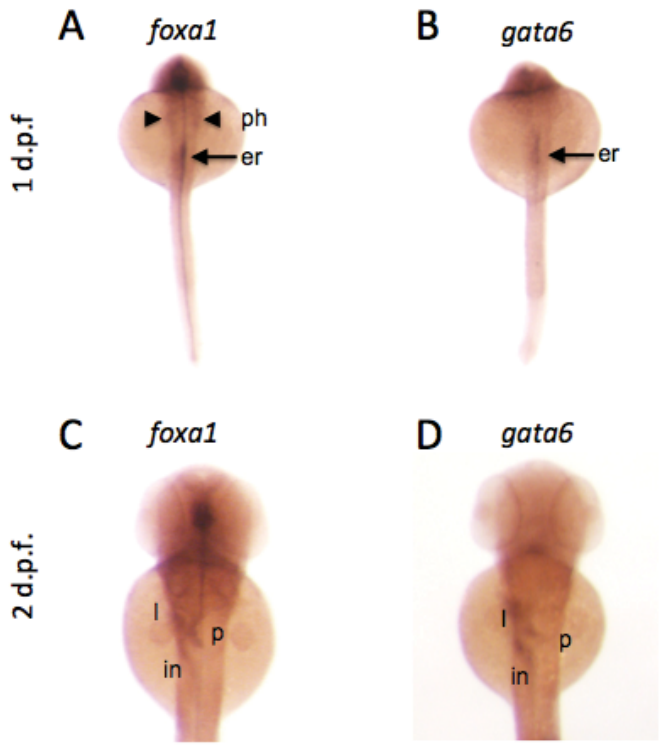

Figure 3-5 Early development of digestive organs is normal in *nol9*^{sa1022} mutants. (A-D) Whole mount *in situ hybridisation* using RNA probes against endoderm marker *foxa1* and *gata6*. Dorsal view with anterior to the top. (A-B) Representative image of all 1 d.p.f. offspring from an incross of *nol9*$^{sa1022/+}$ showing normal expression of *foxa1* (A) and *gata6* (B) in the endodermal rod (er; arrow). The pharyngeal endoderm (ph; arrowhead) also expresses *foxa1* (A). (C-D) Representative image of all 2 d.p.f. offspring from an incross of *nol9*$^{sa1022/+}$ showing expression of *foxa1* (C) and *gata6* (D) in the pancreas (p), liver (l) and intestine (in); (er) endodermal rod; (ph) pharyngeal endoderm; (l) liver; (p) pancreas; (in) intestine.

3.2.5 Expansion growth of the exocrine pancreas and formation of pancreatic ducts are impaired in *nol9*^{sa1022} mutants

To look more specifically at the development of the pancreas, I studied the expression of *pdx1* in 2 d.p.f. offspring from an incross of *nol9*$^{sa1022/+}$ zebrafish and subsequently genotyped the embryos (Figure 3-6 A, Sections 2.1.2 and 2.3.2). All the offspring (n=25) expressed *pdx1* in the pancreatic primordium including nine that were *nol9*^{sa1022} mutants. This data indicates that formation of pancreatic buds proceeds normally in *nol9*^{sa1022} mutants and supports our model that *nol9* is not required for pancreas development before 2 d.p.f.

In order to identify the developmental time point at which pancreas development is affected in *nol9*^{sa1022} mutants, offspring from an incross of *Tg(ins:mCherry)*^{jh2}*;Tg(ptf1a:EGFP)*^{jh1}*;nol9*$^{sa1022/+}$ were phenotyped at either 2, 3, 4 or 5 d.p.f and thereafter genotyped for the *nol9*^{sa1022} mutation (Sections 2.1.2). All 2 d.p.f. (n=24) offspring including seven *nol9*^{sa1022} mutants had formed the pancreatic head comprising of an *insulin*-expressing pancreatic islet surrounded by *ptf1a*-expressing exocrine tissue (Figure 3-6 B). At 3 d.p.f., the pancreatic islet had expanded and the *ptf1a*-expressing region had grown posteriorly in all the 20 embryos studied including four that were *nol9*^{sa1022} mutants (Figure 3-6 C). At 4 d.p.f., the *ptf1a*-positive exocrine pancreas of *nol9*^{sa1022} mutants (n=6) appeared smaller than wild-type siblings (n=14) whereas the *insulin*-positive pancreatic islet was indistinguishable in mutants and wild-type siblings (Figure 3-6 D). At 5 d.p.f., the expansion of the *ptf1a*-expressing region seen in wild-type siblings (n=16) was not visible in *nol9*^{sa1022} mutants (n=6), although the pancreatic islets appeared similar in mutants and wild-type siblings (Figure 3-6 E). These results reveal that the exocrine pancreas in *nol9*^{sa1022} mutants fails to expand normally between 3 and 4 d.p.f. and that this expansion defect is detectable through 5 d.p.f.

To determine whether cell differentiation was normal in the exocrine pancreas of *nol9*^{sa1022} mutants, I studied the production of Carboxypeptidase-a (Cpa), an exocrine pancreatic enzyme by immunohistochemistry (Figure 3-6 F, Section 2.3.3). Cpa was detected in both *nol9*^{sa1022} mutants and wild-type siblings although the Cpa-positive area appeared smaller in mutants compared to wild-type siblings. Overall, these results suggest that the defect in *nol9*^{sa1022} mutants is due to impaired expansion growth rather than impaired cell differentiation of the exocrine pancreas.

Since the expansion of acinar cells of the exocrine pancreas is impaired in *nol9*^{sa1022} mutants, the pancreatic ducts in *nol9*^{sa1022} mutants were examined by immunohistochemistry using an antibody against Cytokeratin labelling the pancreatic ductular epithelia (Figure 3-6 G, Section 2.3.3). At 5 d.p.f., the Cytokeratin-labelled pancreatic ducts of wild-type siblings were highly branched whereas pancreatic ducts were not apparent in *nol9*^{sa1022} mutants. This observation demonstrates that *nol9* is required for the formation of pancreatic ducts in zebrafish.

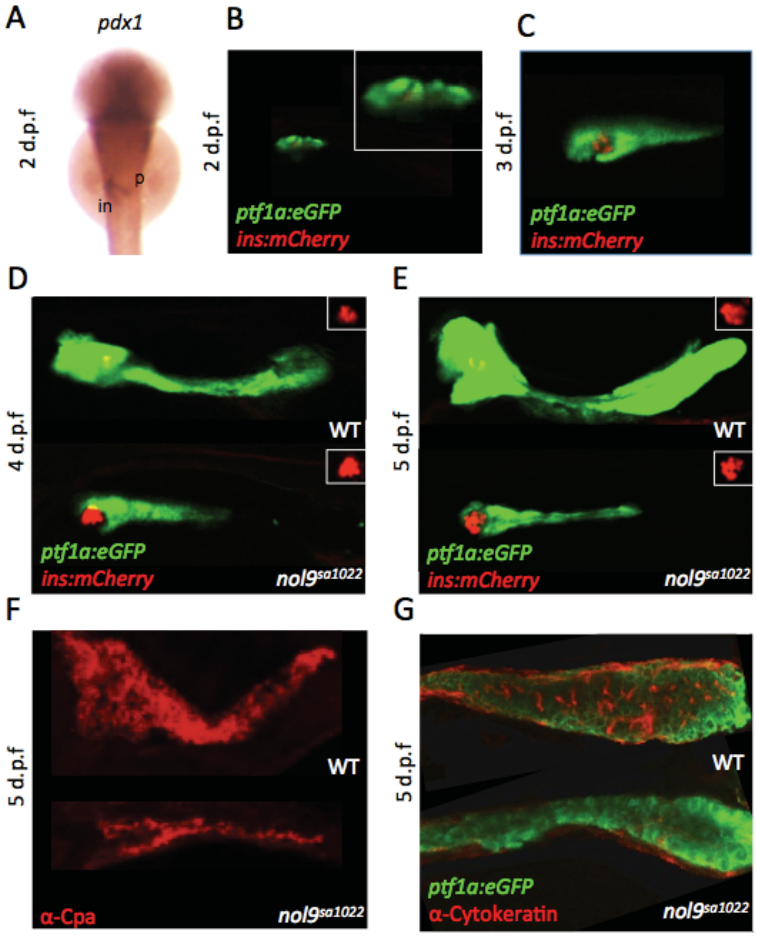

Figure 3-6 Expansion of exocrine pancreas and pancreatic duct formation is impaired in *nol9*^{sa1022} mutants. (A) Dorsal view with anterior to the top. Representative image of 2 d.p.f. offspring from an incross of *nol9*$^{sa1022/+}$ subjected to whole mount *in situ* hybridisation using RNA probes against the pancreas marker *pdx1*. The pancreatic (p) bud forms from the intestine (in). (B-E) 2 d.p.f to 5 d.p.f offspring from an incross of *Tg(ins:mCherry)*^{jh2}*;Tg(ptf1a:EGFP)*^{jh1}*;nol9*$^{sa1022/+}$. (B) Representative image of 2 d.p.f. embryo expressing *insulin* and *ptf1a* (magnified in boxed area). (C) Representative image of 3 d.p.f. embryo showing that the *insulin*- and *ptf1a*-positive region has grown in mutants and wild-type siblings. (D-E) At 4 d.p.f. (D) and 5 d.p.f. (E), the *ptf1a*-expressing exocrine pancreas is smaller in mutants compared to wild-type siblings whereas the *insulin*-expressing pancreatic islet (shown in boxed area) is similar in size in mutants and wild-type siblings. (F) Confocal images of 5 d.p.f. mutants and wild-type siblings subjected to immunohistochemistry using Carboxypeptidase-a (Cpa) antibody. The Cpa-positive area appears smaller in mutants compared to wild-type siblings. (G) Representative maximum intensity projection images of confocal stacks of 5 d.p.f. larvae from an incross of *Tg(ins:mCherry)*^{jh2}*;Tg(ptf1a:EGFP)*^{jh1}*;nol9*$^{sa1022/+}$ expressing only EGFP and subjected to immunohistochemistry using antibody against Cytokeratin. The pancreatic ducts are not apparent in *nol9*^{sa1022} mutants and is in contrast to the ductal network labelled in wild-type siblings. (WT) wild-type; (p) pancreas; (in) intestine.

3.2.6 Pancreatic endocrine cells are formed and are differentiated in *nol9*^{sa1022} mutants

As the *nol9*^{sa1022} mutants appeared to have similar *insulin*-expressing area as wild-type siblings, the pancreatic endocrine cells were studied at earlier stages by immunohistochemistry on offspring from an incross of *Tg(ins:mCherry)*^{jh2}*;Tg(ptf1a:EGFP)*^{jh1}*;nol9*$^{sa1022/+}$ adults (Figure 3-7, Section 2.3.3). At 2 d.p.f., *nol9*^{sa1022} mutants (n=16) and wild-type siblings (n=25) had similar levels of Pdx1 that labelled both the pancreatic islet and the exocrine tissue, and the area of Glucagon α-cells in *nol9*^{sa1022} mutants was indistinguishable from that in wild-siblings (Figure 3-7 A-D). In addition, *nol9*^{sa1022} mutants (n=4) showed a comparable area of Insulin-producing β-cells as wild-type siblings (n=24) (Figure 3-7 E). Moreover, the area of Somatostatin-producing δ-cells was similar between *nol9*^{sa1022} mutants (n=10) and wild-type siblings (n=22) (Figure 3-7 F). These results suggest that before 2 d.p.f., the formation and differentiation of endocrine cells proceed normally in *nol9*^{sa1022} mutants. At 4 d.p.f., the area of *ins:mcherry* cells is comparable between *nol9*^{sa1022} mutants (n=14) and wild-type siblings (n=15) (Figure 3-7 G, J). Similarly, the area of Somatostatin-producing and Glucagon-producing cells is not distinguishable between *nol9*^{sa1022} mutants (n=13 for Somatostatin and Glucagon) and wild-type siblings (n=13 for Somatostatin and n=16 for Glucagon) (Figure 3-7 H, K, I, L). These data suggest that the pancreatic endocrine cells of *nol9*^{sa1022} mutants continue to develop normally. Altogether, these observations indicate that the pancreatic endocrine cells form and differentiate into α-, β- and γ- cells in *nol9*^{sa1022} mutants and that the loss of *nol9* does not impair the development of the pancreatic islet.

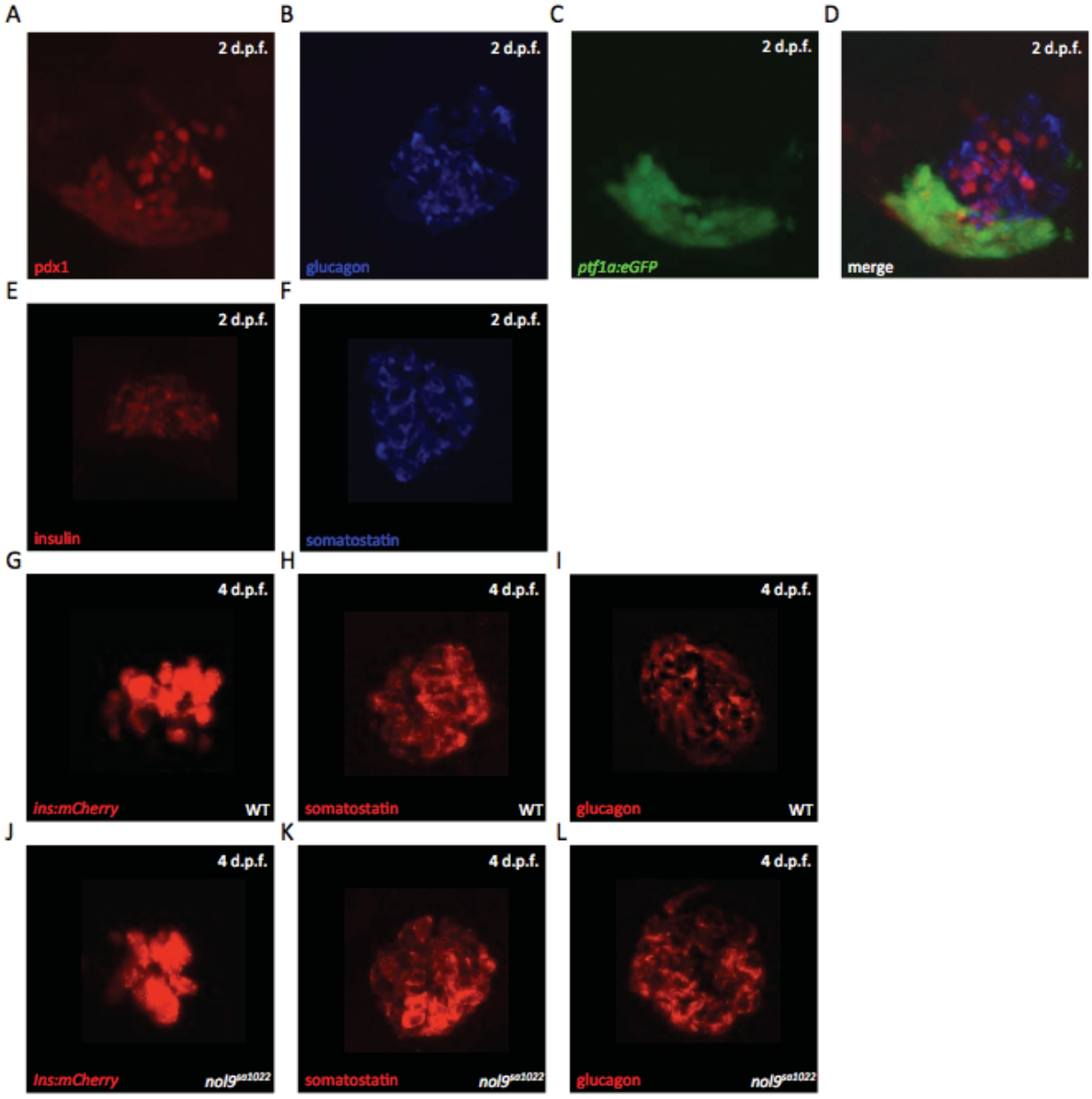

Figure 3-7 Formation and differentiation of pancreatic endocrine cells proceed normally in *nol9*^{sa1022} mutants. (A-L) Offspring from an incross of *Tg(ins:mCherry)*^{jh2}*;Tg(ptf1a:EGFP)*^{jh1}*;nol9*$^{sa1022/+}$; A-F, H, I, K and L express *EGFP* only and have been subjected to immunohistochemistry. (A-D) Representative image of 2 d.p.f. embryo showing presence of Pdx1-producing cells (A), Glucagon-producing cells (B), *ptf1a*-expressing cells (C) and a merged image (D). (E-F) Representative image of 2 d.p.f. offspring showing Insulin- (E) and Somatostatin- (F) producing cells. (G-L) 4 d.p.f. larvae showing comparable levels of *insulin* expression (G, J), Somatostatin (H, K) and Glucagon (I, L) between *nol9*^{sa1022} mutants (J, K, L) and wild-type siblings (G, H, I). (WT) wild-type.

3.2.7 Secondary islets cells expressing *insulin* are present in *nol9*^{sa1022} mutants

In order to study secondary islet formation in *nol9*^{sa1022} mutants, offspring from an incross of *Tg(ins:mCherry)*^{jh2}*;Tg(ptf1a:EGFP)*^{jh1}*;nol9*$^{sa1022/+}$ were incubated from 3 to 5 d.p.f. in egg water containing PTU with either 100 μM of Notch inhibitor *N*-[*N*-(3,5-difluorophenacetyl)-L-alanyl]-*S*-phenylglycine *t*-butyl ester (DAPT), Dimethyl sulfoxide (DMSO) or left untreated (Figure 3-8, Section 2.4.2). At 5 d.p.f., the percentage of untreated *nol9*^{sa1022} mutants and wild-type siblings that had *insulin*-positive secondary islets were 57.9% (11 out of 19) and 33.3% (5 out of 15) respectively (Figure 3-8 A, B). For DMSO-treated larvae, 31.3% (5 out of 16) *nol9*^{sa1022} mutants and 37.5% (6 out of 16) wild-type siblings had *insulin*-expressing secondary islets. The percentage of DAPT-treated *nol9*^{sa1022} mutants and wild-type siblings that had secondary islets were 71.4% (10 out of 14) and 72.4% (21 out of 29) respectively, both higher than DMSO-treated and untreated larvae. This data suggests that DAPT increases the percentage of larvae with secondary islets in both *nol9*^{sa1022} mutants and wild-type siblings. The mean number of secondary islets was 0.79 and 0.47 for untreated *nol9*^{sa1022} mutants and wild-type siblings respectively (Figure 3-8 C). The DMSO-treated *nol9*^{sa1022} mutants and wild-type siblings also had the same mean number of secondary islets of 0.625. Similarly, the mean number of secondary islets for DAPT-treated larvae was higher compared to DMSO-treated and untreated larvae (1.5 for *nol9*^{sa1022} mutants and 1.79 for wild-type siblings). The mean number of secondary islets in wild-type siblings in DAPT treatment was statistically significantly higher than that in DMSO treatment (Student's *t*-test, $p = 0.015$) and without treatment (Student's *t*-test, $p = 0.005$). The mean number of secondary islets in *nol9*^{sa1022} mutants in DAPT treatment was not statistically significantly different from that in DMSO treatment (Student's *t*-test, $p = 0.065$) or without treatment (Student's *t*-test, $p = 0.088$). These results indicate that the mean number of secondary islets in *nol9*^{sa1022} mutants is similar to wild-type siblings when left untreated or treated with DAPT or DMSO. Overall, this experiment demonstrates that secondary islet cells expressing *insulin* are formed in *nol9*^{sa1022} mutants and that together with results from the previous section suggest that the *nol9* mutation does not impair the development of the endocrine pancreas.

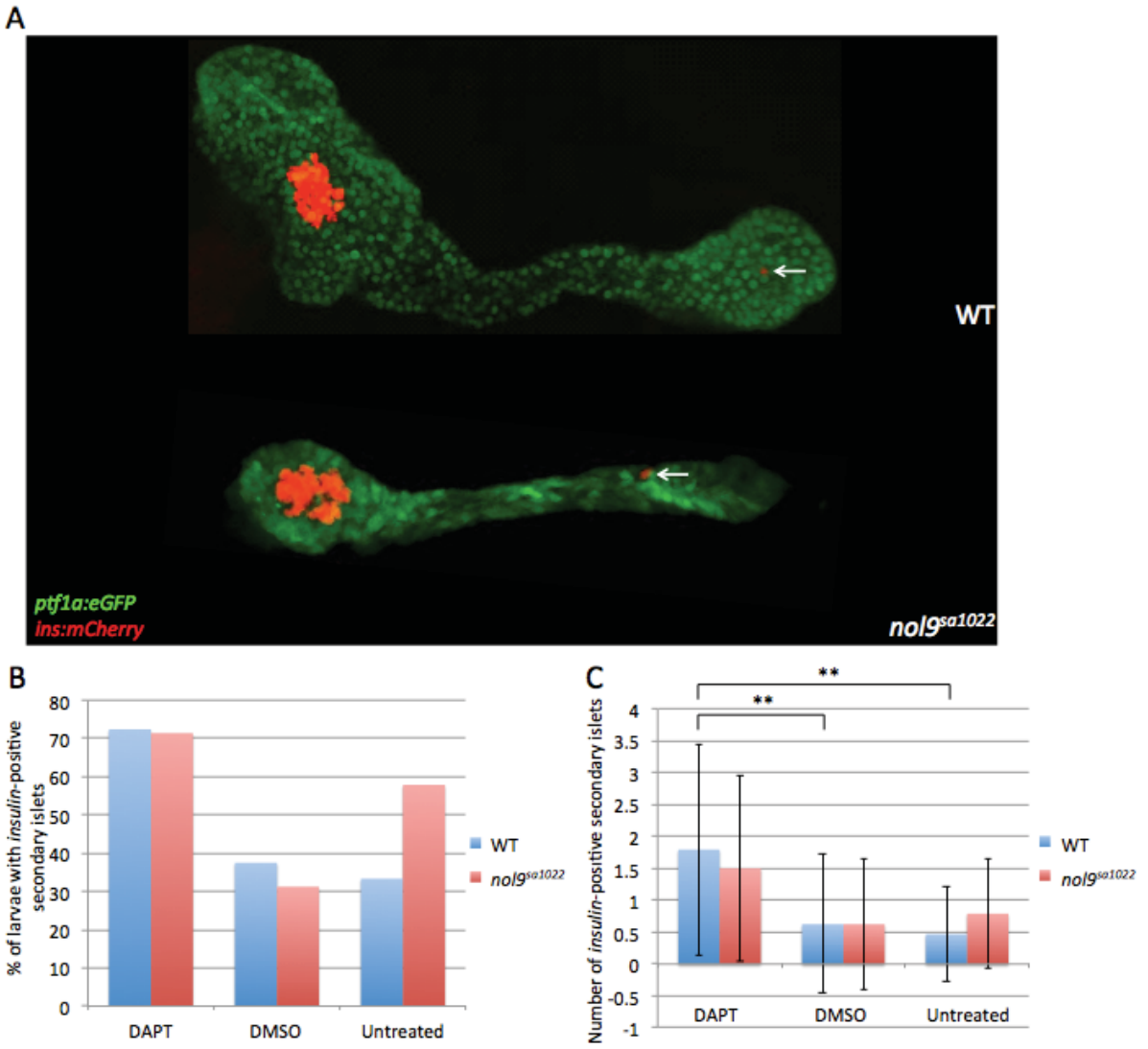

Figure 3-8 Secondary islet cells expressing *insulin* are formed in *nol9*^{sa1022} mutants. (A) Representative maximum intensity projection images of confocal stacks of 5 d.p.f. larvae from an incross of *Tg(ins:mCherry)*^{jh2}*;Tg(ptf1a:EGFP)*^{jh1}*;nol9*$^{sa1022/+}$ showing presence of *insulin*-positive secondary islets (arrow) in both *nol9*^{sa1022} mutants and wild-type siblings. (B) Graph showing the percentage of 5 d.p.f. untreated, DMSO-treated or DAPT-treated *nol9*^{sa1022} mutants and wild-type siblings that displayed *insulin*-positive secondary islets. (C) Graph showing the mean number of *insulin*-positive secondary islets of untreated, DMSO-treated or DAPT-treated *nol9*^{sa1022} mutants and wild-type siblings. Data is represented as the mean ± SD, Student's *t*-test **p<0.01. (WT) wild-type.

3.2.8 Expansion growths of liver and intestine are impaired in *nol9^{sa1022}* mutants

The endodermally-derived organs liver and intestine were found to be underdeveloped in *nol9^{sa1022}* mutants under the dissecting microscope. To examine the development of the liver, I studied the expression of *prospero homeobox protein 1* (*prox1*), an early hepatocyte marker (Glasgow and Tomarev, 1998), in offspring from an incross of *nol9$^{sa1022/+}$* from 2 d.p.f. to 4 d.p.f. and then genotyped them for the *nol9^{sa1022}* mutation (Sections 2.1.2 and 2.3.2). All 2 d.p.f embryos (n=26) expressed *prox1* in the liver primordium, including two that were *nol9^{sa1022}* mutants (Figure 3-9 A). At 3 d.p.f., all the offspring showed normal expression of *prox1* in the liver and seven of all the 37 offspring studied were *nol9^{sa1022}* mutants (Figure 3-9 B). At 4 d.p.f. however, the *nol9^{sa1022}* mutants (n=9) could be distinguished from wild-type siblings (n=26) as having a smaller *prox1*-expressing region (Figure 3-9 C). This data suggests that *nol9* is not required for the initiation and budding of the liver but for its expansion between 3 and 4 d.p.f.

The development of the intestine of *nol9^{sa1022}* mutants was followed by studying the expression of the intestinal epithelium marker *fatty acid binding protein 2* (*fabp2*) in offspring from *nol9$^{sa1022/+}$* zebrafish at 3 d.p.f. and 4 d.p.f (Andre et al., 2000) (Sections 2.1.2 and 2.3.2). All 3 d.p.f. offspring expressed *fabp2* in the foregut and nine out of 49 embryos studied were *nol9^{sa1022}* mutants (Figure 3-9 D). At 4 d.p.f., the *nol9^{sa1022}* mutants (n=11) showed a smaller *fabp2*-expressing region compared to wild-type siblings (n=22) (Figure 3-9 E). This data suggests that the *nol9^{sa1022}* mutation does not abolish cell differentiation in the intestine but instead affects the expansion growth of the intestine between 3 and 4 d.p.f.

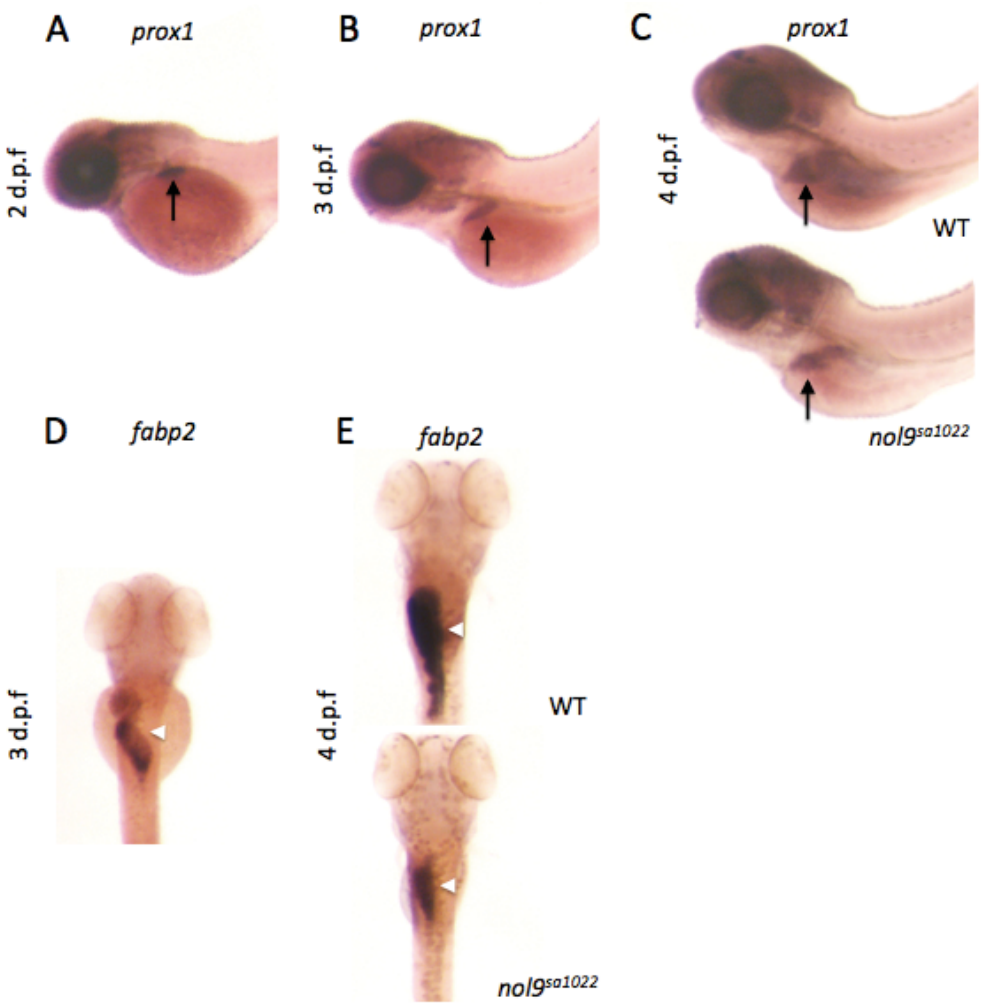

Figure 3-9 Expansion growths of liver and intestine are impaired in *nol9*^{sa1022} mutants. (A-E) Whole mount *in situ* hybridisation using RNA probes against *prox1* (A-C) and *fabp2* (D-E) on offspring from incross of *nol9*$^{sa1022/+}$ zebrafish. (A-C) Lateral view with anterior to the left. (A-B) Representative image of 2 d.p.f. (A) and 3 d.p.f. (B) offspring showing expression of *prox1* in the liver (arrow). (C) At 4 d.p.f., *nol9*^{sa1022} mutants have a smaller *prox1*-expressing region (arrow) compared to wild-type siblings. (D-E) Dorsal view with anterior to the top. (D) Representative image of 3 d.p.f. offspring showing expression of *fabp2* in the intestine (arrowhead). (E) 4 d.p.f. *nol9*^{sa1022} mutants have a smaller *fabp2*-positive region compared to wild-type siblings. (WT) wild-type.

3.2.9 The *nol9*^{sa1022} mutants have different proportion of cells in *G1*, *S* and *G2* phases of cell cycle

The expansion defects of digestive organs in *nol9*^{sa1022} mutants could be explained by two different hypotheses. Firstly, the proliferation of cells of digestive organs may be impaired in *nol9*^{sa1022} mutants. Secondly, there may be an increase in cell death in the digestive organs. To study cell proliferation of *nol9*^{sa1022} mutants, I first analysed the cell cycle of *nol9*^{sa1022} mutants by flow cytometry with propidium iodide to measure the proportion of cells in different phases of the cell cycle (Section 2.4.3). Four biological replicates of 5 d.p.f. *nol9*^{sa1022} mutants and wild-type larvae pairs were obtained with an equal number of larvae (70-100) for each pair. There was a significant increase in the percentage of cells in *G1* phase in *nol9*^{sa1022} mutants (97.1%) compared to wild-type siblings (95.5%) according to the Student's *t*-test ($p = 2.5\text{x}10^{-6}$) (Figure 3-10). This was accompanied by a significant decrease in the percentage of cells in *S* phase in *nol9*^{sa1022} mutants (1.6%) compared to wild-type siblings (2.6%, Student's *t*-test, $p = 2.5\text{x}10^{-5}$). The percentage of cells in *G2* phase in mutants (1.3%) was significantly smaller than those in wild-type siblings (1.8%, Student's *t*-test, $p = 6.3\text{x}10^{-5}$). These results indicate that cell proliferation is impaired in *nol9*^{sa1022} mutants and could contribute to the defective expansion of digestive organs.

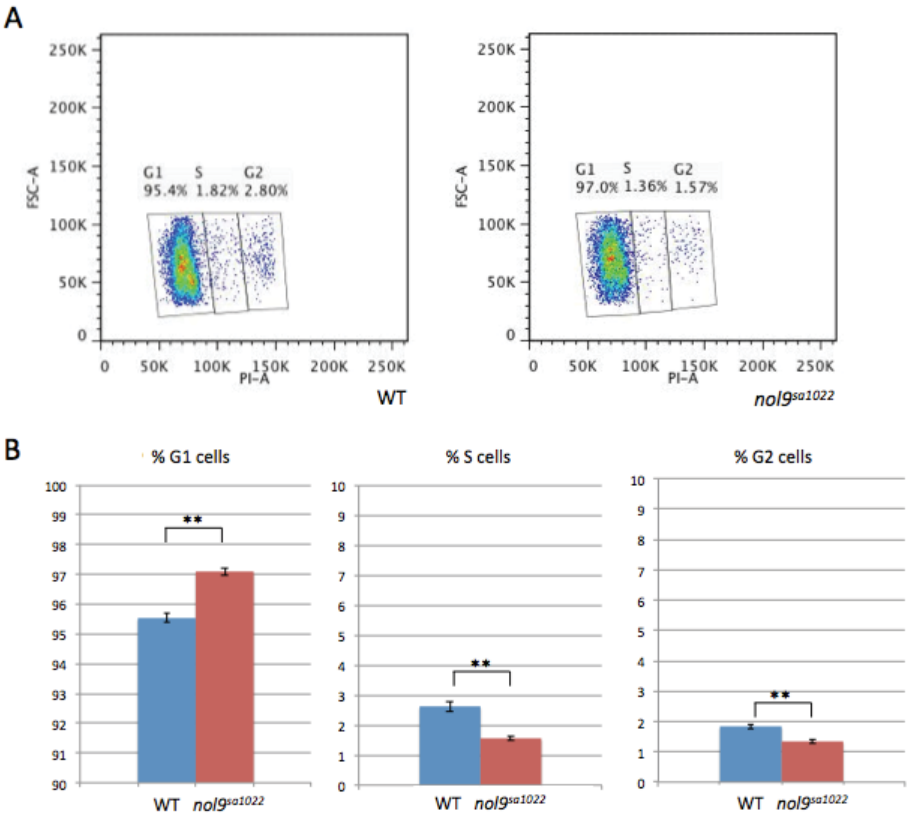

Figure 3-10 Cell cycle analysis of 5 d.p.f. *nol9*^{sa1022} mutants and wild-type siblings. (A) Representative scatter plots of propidium iodide (PI) staining versus forward scatter (FSC) of cells from wild-type (left) and *nol9*^{sa1022} mutant (right). (B) Graph of proportion of cells in G1, S and G2 cell cycle phases in wild-type and *nol9*^{sa1022} mutants. Data from four biological replicates is represented as the mean ± SD, Student's *t*-test **p<0.01. (WT) wild-type.

3.2.10 The pancreas of *nol9*^{sa1022} mutants show impaired cell proliferation

In order to examine cell proliferation in the pancreas of *nol9*^{sa1022} mutants, I measured 5-bromo-2'-deoxyuridine (BrdU) incorporation in 4 d.p.f. larvae from an incross of *Tg(ins:mCherry)*^{jh2}*;Tg(ptf1a:EGFP)*^{jh1}*;nol9*$^{sa1022/+}$ expressing only EGFP and not mCherry (Figure 3-11, Section 2.4.4). The mean number of *ptf1a*-expressing cells that were positive for BrdU was statistically significantly smaller in *nol9*^{sa1022} mutants, 19.33 (n=9) than that in wild-type siblings, 44.14 (n=7) according to the Student's *t*-test, $p = 0.00011$ (Figure 3-11 A, B, E). In contrast, the mean number of cells that were positive for BrdU in the spinal cord region above the vent is not statistically significantly different in *nol9*^{sa1022} mutants, 78.3 (n=3) and wild-type siblings, 78 (n=3) (Student's *t*-test, $p = 0.972$) (Figure 3-11 C, E). Similarly, the mean number of BrdU-positive cells in the spinal cord near the tail is comparable in *nol9*^{sa1022} mutants, 55.3 (n=3) and wild-type siblings, 55 (n=6) (Student's *t*-test, $p = 0.709$) (Figure 3-11 D, E). These results indicate that the proliferation rate of pancreatic exocrine cells is reduced in *nol9*^{sa1022} mutants and that impaired cell proliferation contributes to the expansion defect of the pancreas in *nol9*^{sa1022} mutants.

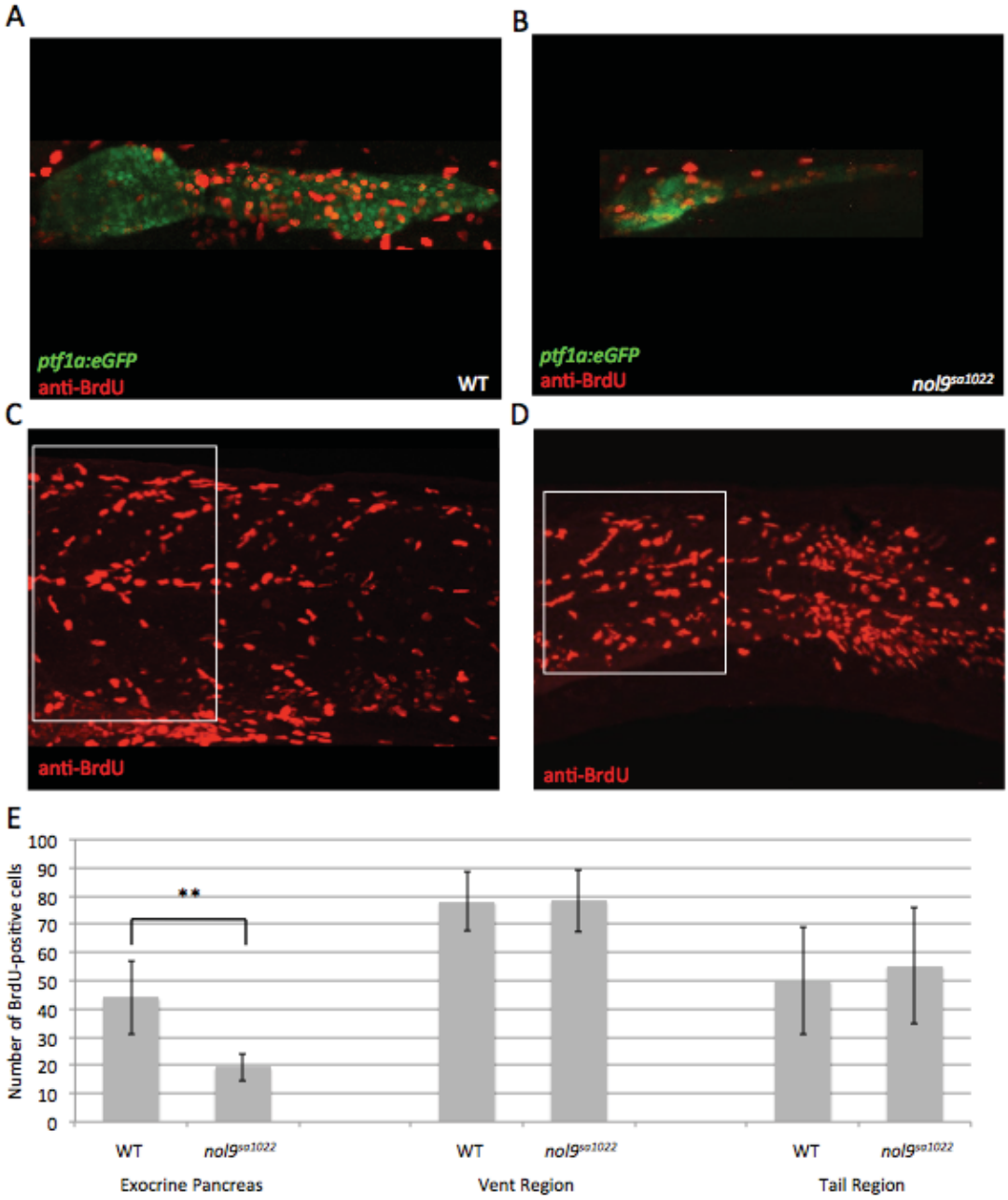

Figure 3-11 The cell proliferation of the exocrine pancreas of *nol9*^{sa1022} mutants is impaired. (A-D) Representative maximum intensity projection images of a z series of confocal sections through 4 d.p.f. larvae from an incross of *Tg(ins:mCherry)*^{jh2}*;Tg(ptf1a:EGFP)*^{jh1}*;nol9*$^{sa1022/+}$ expressing only EGFP and subjected to BrdU incorportation assay. (A-B) The number of BrdU-positive cells is smaller in *nol9*^{sa1022} mutants (B) compared to wild-type siblings (A). (C-D) Representative maximum intensity projection images of confocal stacks of the spinal cord region (boxed area) above the vent (C) and near the tail (D) where the number of BrdU-positive cells was counted. (E) Graph showing that the number of BrdU-positive cells in the exocrine pancreas of *nol9*^{sa1022} mutants (n=9) is statistically significantly smaller than that of wild-type siblings (n=7). The number of BrdU-positive cells in the spinal cord region above the vent and near the tail is similar in both *nol9*^{sa1022} mutants (n=3 for both regions) and wild-type siblings (n=3 for vent region and n=6 for tail region). Data is represented as the mean ± SD, Student's *t*-test **p<0.01. (WT) wild-type.

3.2.11 The pancreas of *nol9*^{sa1022} mutants do not show increased cell death

In addition to impaired cell proliferation, an increase in cell death could also contribute to the expansion defect of the exocrine pancreas in *nol9*^{sa1022} mutants. Therefore, cell death was studied using the terminal deoxynucleotidyl transferase dUTP nick end labelling (TUNEL) staining on 4 d.p.f. larvae from an incross of *Tg(ins:mCherry)*^{jh2}*;Tg(ptf1a:EGFP)*^{jh1}*;nol9*$^{sa1022/+}$ expressing only EGFP and not mCherry (Figure 3-12, Section 2.4.5). There were no tetramethylrhodamine (TMR)-labelled apoptotic cells in the pancreas of *nol9*^{sa1022} mutants (n=8) and wild-type siblings (n=9) (Figure 3-12 A). The mean number of apoptotic cells in the tails of *nol9*^{sa1022} mutants and wild-type siblings were not statistically significantly different, 14 and 11.4 respectively (Student's *t*-test, p = 0.179) (Figure 3-12 B, C). This experiment demonstrates that increase in cell death does not contribute to the expansion defect of the exocrine pancreas in *nol9*^{sa1022} mutants.

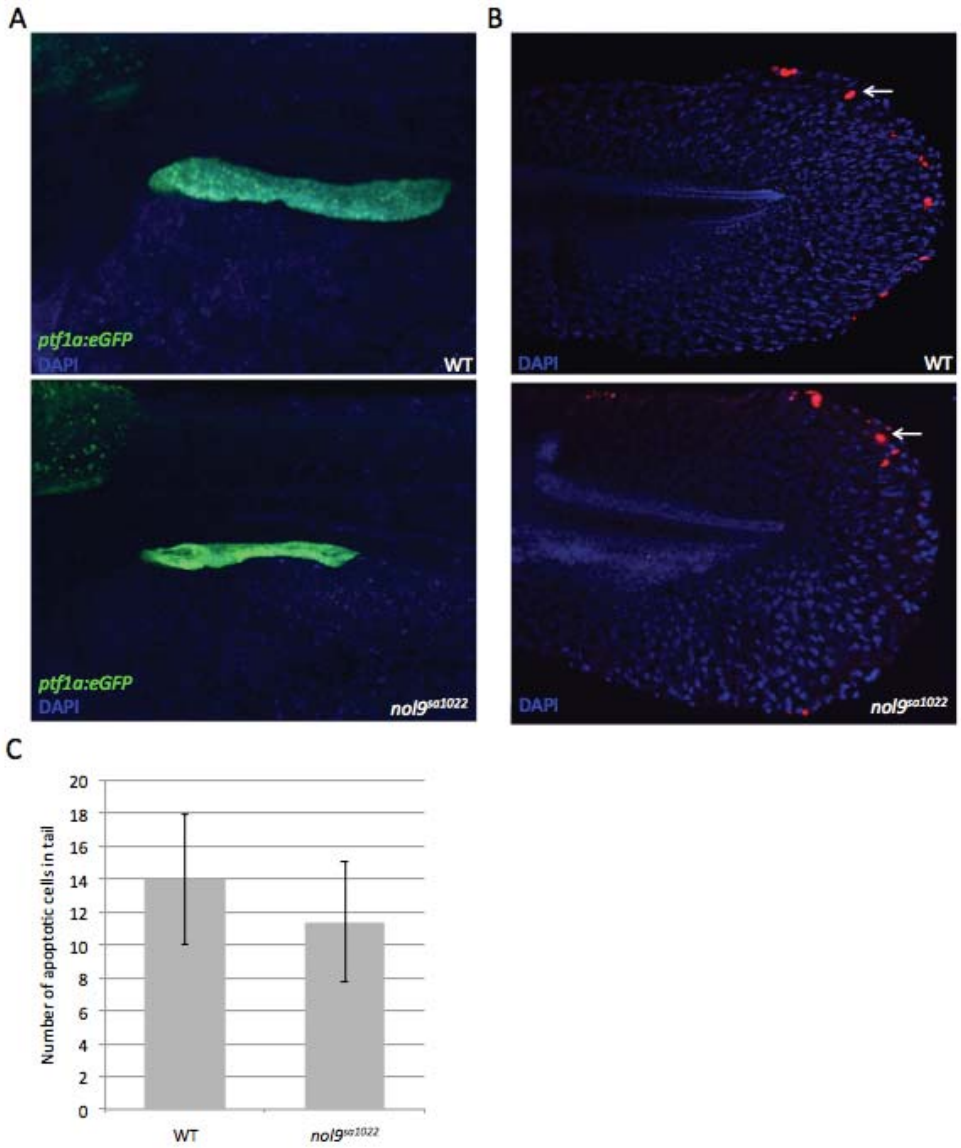

Figure 3-12 The exocrine pancreas of *nol9*^{sa1022} mutants do not show an increase in cell death. (A-B) Maximum intensity projection images of a z series of confocal sections through 4 d.p.f. larvae from an incross of *Tg(ins:mCherry)*^{jh2}*;Tg(ptf1a:EGFP)*^{jh1}*;nol9*$^{sa1022/+}$ expressing only EGFP and subjected to TUNEL and DAPI staining. (A) There are no TMR-labelled apoptotic cells in *ptf1a*-expressing exocrine pancreas of *nol9*^{sa1022} mutants and wild-type siblings. (B) The tails of *nol9*^{sa1022} mutants and wild-type siblings have apoptotic cells (arrow). (C) The mean number of apoptotic cells in the tails of *nol9*^{sa1022} mutants (n=8) is not statistically significantly different from those of wild-type siblings (n=9). Data is represented as the mean ± SD. (WT) wild-type.

3.2.12 Development of the jaw cartilage and erythrocyte is normal in *nol9*^{sa1022} mutants

Craniofacial dysmorphology is a common feature of ribosomopathies (Narla and Ebert, 2010) and previously described zebrafish mutants in genes *rbm19* (Mayer and Fishman, 2003), *def* (Chen et al., 2005), *pwp2h* (Boglev et al., 2013) and *nom1* (Qin et al., 2014) all exhibit abnormal craniofacial development. At 5 d.p.f., there were no major differences between the jaw of *nol9*^{sa1022} mutants and wild-type siblings under a dissecting microscope. To characterise the jaw of *nol9*^{sa1022} mutants further, 5 d.p.f. *nol9*^{sa1022} mutants and wild-type siblings were subjected to Alcian blue staining that labels acidic polysaccharides present in cartilages (Section 2.4.2). In zebrafish, the pharyngeal cartilage consists of seven pharyngeal arches: the anterior two form the jaw whilst the posterior five form the gill structures (Neuhauss et al., 1996). All the jaw cartilage elements were present and appeared normal in *nol9*^{sa1022} mutants (n=23) and wild-type siblings (n=54) (Figure 3-13 A). They include the first phargyngeal arch derivatives, Meckel's cartilage and palatoquadrate, the second pharyngeal arch derivative ceratohyal, and the third and seventh pharyngeal arches, namely the five ceratobranchials (Figure 3-13 A). This data suggests that *nol9*^{sa1022} mutants have normal jaw and branchial arch structures and that *nol9* is not required for craniofacial development.

A haematological phenotype such as anaemia is a shared clinical feature of ribosomopathies (Narla and Ebert, 2010). In both teleosts and mammals, haematopoiesis occurs in four sequential waves. The first two primitive waves produce transient precursors giving rise to embryonic macrophages and erythrocytes whilst the next two definitive waves consist of multipotent progenitors of adult cell types including firstly the erythromyeloid progenitors (EMPs) that will give rise to erythroid and myeloid lineages and then the multipotent haematopoietic stem cells (HSCs) which can produce all adult haematopoietic cell types and self renew (Stachura and Traver, 2011). The haemotopoietic cells of the definitive wave first appear around 26 h.p.f. in the aorta-gonad-mesonephros region and later seed the caudal hematopoietic tissue, where they expand and differentiate (Bertrand et al., 2010). Definitive erythrocytes derived from haematopoietic stem cells appear in the caudal haematopoietic tissue at 3 d.p.f. and slowly replace primitive erythrocytes in circulation (Chen and Zon, 2009). The formation of erythrocytes during early development was studied in *nol9*^{sa1022} mutants to investigate whether *nol9*^{sa1022} mutants also exhibited an anaemic

phenotype. All offspring from an incross of *nol9*$^{sa1022/+}$ zebrafish showed normal blood circulation in the heart and tail at 3 d.p.f. and 5 d.p.f. under the dissecting microscope. All 3 d.p.f. offspring showed a similar area of primitive erythrocytes that were stained with o-dianisidine; 18 out of the 70 zebrafish studied were *nol9*^{sa1022} mutants (Figure 3-13 B, Section 2.4.7). At 5 d.p.f., the presence of haemoglobin-containing erythrocytes was evident in both *nol9*^{sa1022} mutants (n=18) and wild-type siblings (n=51) (Figure 3-13 C). These results indicate that *nol9* is not required for the production of primitive erythrocytes during early development in zebrafish.

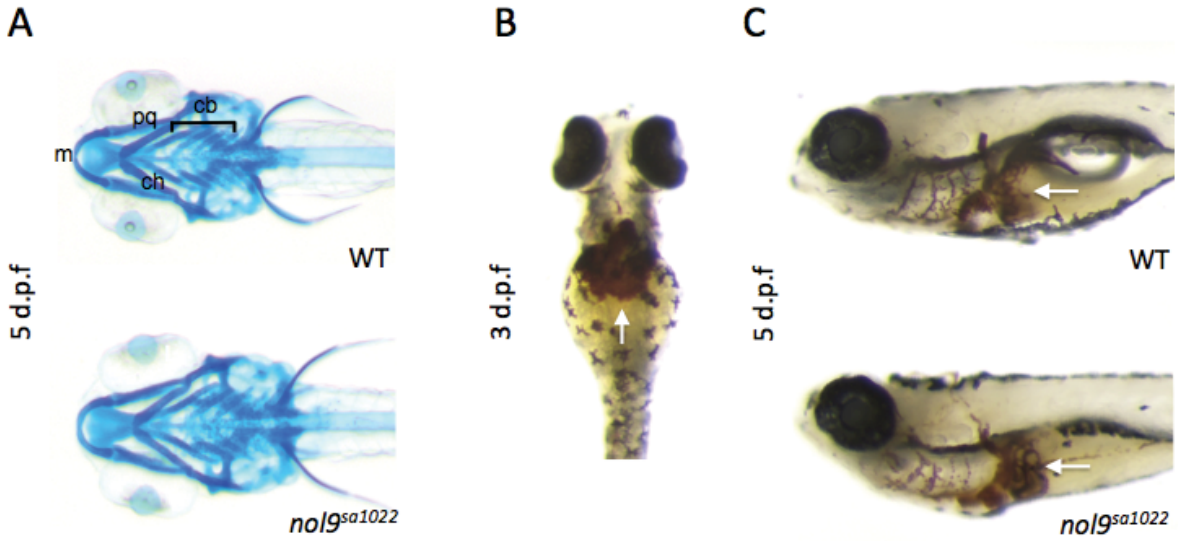

Figure 3-13 Development of jaw cartilage and erythrocyte is normal in *nol9*^{sa1022} mutants. (A) Ventral view with anterior to the left. Alcian blue staining revealed the normal formation of the jaw cartilage elements Meckel's (m), palatoquadrate (pq), ceratohyal (ch) and ceratobranchial (cb) in both *nol9*^{sa1022} mutants and wild-type siblings. (B) Ventral view with anterior to the top. Representative image of all 3 d.p.f. offspring from an incross of *nol9*$^{sa1022/+}$ labelling haemoglobin-containing erythrocytes (arrow). (C) Left side view of 5 d.p.f. wild-type and *nol9*^{sa1022} mutants showing the presence of erythrocytes (arrow) stained with o-dianisidine. (WT) wild-type; (m) meckel's; (pq) palatoquadrate; (ch) ceratohyal; (cb) ceratobranchials.

3.2.13 Developmental expression pattern of *nol9*

The defects in *nol9*^{sa1022} mutants were restricted to specific tissues despite the gene's crucial role in ribosome biogenesis, a process that is required in all tissues. In order to explain the tissue specificity of the phenotype, the expression of *nol9* during development was investigated. RNA-seq data from Ensembl revealed that *nol9* is maternally expressed at the 2-cell stage, and is also expressed at the different developmental stages studied 1, 2, 3 and 5 d.p.f. (Collins et al., 2012; Harvey et al., 2013). In order to examine the expression patterns of *nol9* during development, whole mount *in situ* hybridisation (WISH) was carried out using DIG-labelled RNA probe against *nol9* mRNA on PTU-treated wild-type zebrafish at different stages of development (Section 2.3.2). There was strong expression of *nol9* at 3 hours post fertilisation (h.p.f.), (Figure 3-14 A) and by 1 d.p.f., *nol9* was ubiquitously expressed with high levels detected in the head, eye and notochord (Figure 3-14 B). At 3 d.p.f., the expression became restricted to specific organs namely pancreas, liver, intestine and head (Figure 3-14 C) and this expression pattern continued to 4 d.p.f. (Figure 3-14 D). At 5 d.p.f., *nol9* was still strongly expressed in the digestive organs and was also expressed in the otic vesicles (Figure 3-14 E). The expression data reveals that *nol9* is initially ubiquitously expressed but then becomes restricted to specific organs including the pancreas, liver and intestine.

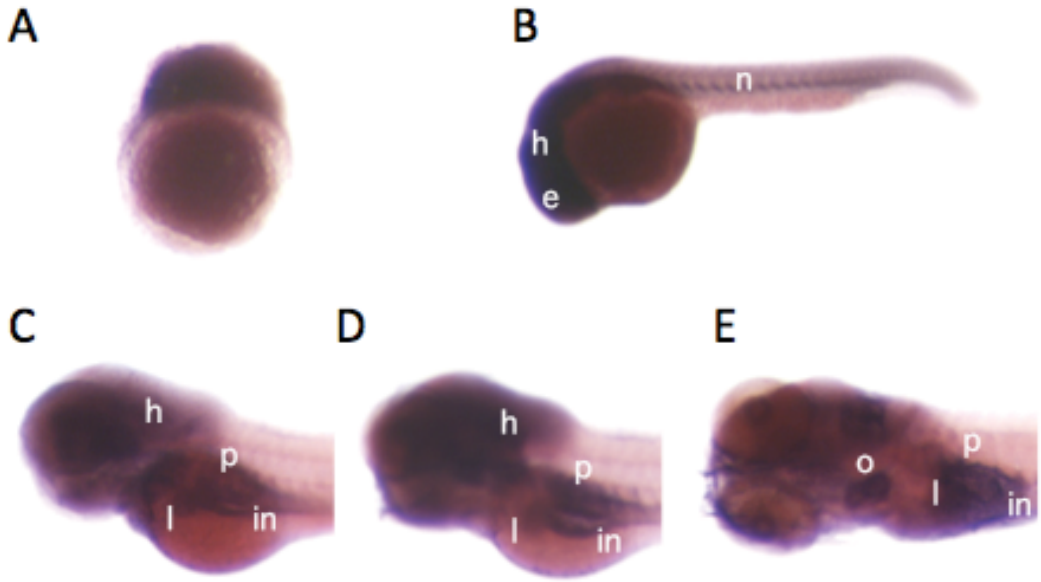

Figure 3-14 Developmental expression pattern of *nol9*. (A) Lateral view of 3 h.p.f. embryo showing strong *nol9* expression. (B-E) Lateral view with anterior to the left. (B) At 1 d.p.f., *nol9* is ubiquitously expressed with strong expression in the head, notochord and eye. (C-D) At 3 d.p.f. (C) and 4 d.p.f. (D), expression of *nol9* is apparent in the head, liver, pancreas and intestine. (E) At 5 d.p.f., *nol9* is strongly expressed in the digestive organs and also in the otic vesicles. (h) head; (n) notochord; (e) eye; (p) pancreas; (l) liver; (in) intestine; (o) otic vesicles.

3.2.14 The processing of 28S rRNA is impaired in *nol9*^{sa1022} mutants

Previous work demonstrated that human NOL9 protein is required for rRNA processing and more specifically for the generation of 5.8S and 28S rRNAs (Heindl and Martinez, 2010). To investigate whether Nol9 plays a similar role in zebrafish, incrosses of *Tg(ins:mCherry)*^{jh2}*;Tg(ptf1a:EGFP)*^{jh1}*;nol9*$^{sa1022/+}$ were phenotyped at 5 d.p.f based on the size of the *ptf1a*-expressing region. Northern blot analysis was carried out in collaboration with Dr Tobias Fleischmann on RNA of *nol9*^{sa1022} mutants and wild-type siblings from two biological replicates using a probe designed against the sequence spanning the 5.8S and Internal Transcriped Spacer (ITS)-2 (Sections 2.2 and 2.5.1) (Figure 3-15 A). RNAse H was used to digest a region of ~ 400 nucleotides (nts) from the start of the 28S rRNA sequence to distinguish between the different precursors that generate the mature 5.8S and 28S rRNAs Figure 3-15). Figure 3-15 A shows a schematic of rRNA processing including some of the different rRNA intermediates (Azuma et al., 2006). In the digested RNA from *nol9*^{sa1022} mutants, a band of 1000 nts displayed increased signal compared to that of digested RNA from wild-type siblings. This band corresponds to rRNA intermediate A (Figure 3-15 A, B). Additionally, two smaller bands of ~ 700 nts had signal of higher intensity in *nol9*^{sa1022} mutants RNA compared to those of wild-type RNA. These two bands correspond to rRNA intermediates B and C (Figure 3-15 A, B). The intensity of the 5.8S bands appeared similar in *nol9*^{sa1022} mutants and wild-type siblings. These data suggest that there is an accumulation of rRNA intermediates that generate 5.8S and 28S rRNA in *nol9*^{sa1022} mutants.

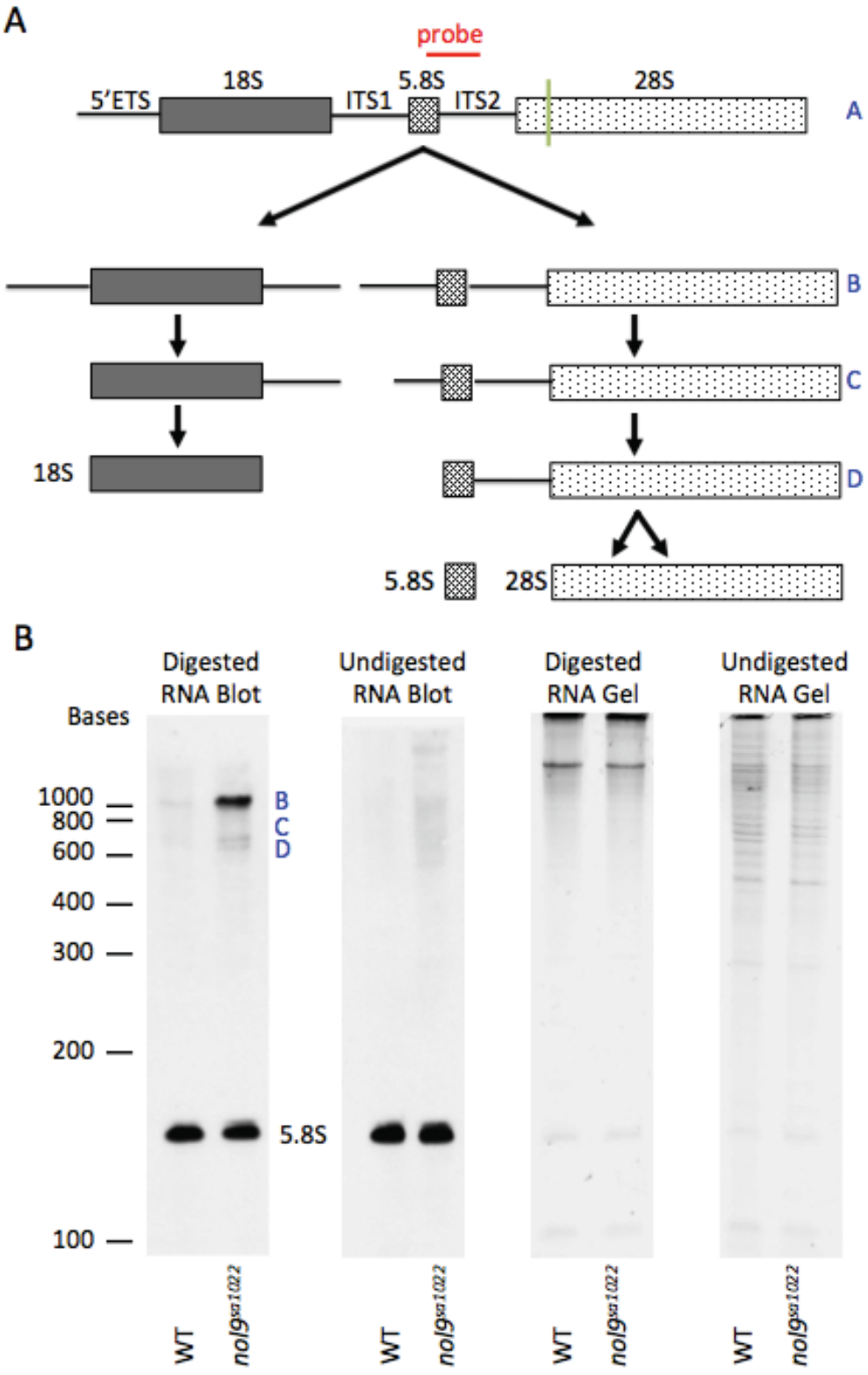

Figure 3-15 rRNA processing is impaired in *nol9*^{sa1022} mutants. (A) Schematic representation of the rRNA processing pathway. The site of hybridisation of the 5.8S-ITS2 probe (red) and the site where RNA was digested (green) are indicated. (B) Representative Northern blot analysis of RNA isolated from 5 d.p.f. *nol9*^{sa1022} mutants and wild-type siblings using the 5.8S-ITS2 probe to detect rRNA processing intermediates (blue). In the digested RNA blot, there is a marked increase in rRNA intermediate A of 1000 nts and an increase in rRNA intermediates B and C of ~ 700 nts in *nol9*^{sa1022} mutants compared to wild-type siblings. There was no apparent difference in the 5.8S band between in *nol9*^{sa1022} mutants compared to wild-type siblings. The RNA gel shows that equal amounts of RNA was loaded in *nol9*^{sa1022} mutants compared to wild-type siblings (WT) wild-type.

To determine if the ratio of 28S to 18S was altered in *nol9*^{sa1022} mutants RNA was compared on a bioanalyser (Section 2.2 and 2.5.1). The level of mature 28S rRNA in *nol9*^{sa1022} mutants was reduced compared to wild-type siblings, whereas levels of mature 18S rRNA were similar (Figure 3-16 A). These differences altered the 28S/18S rRNA ratio, which was 1.78 in *nol9*^{sa1022} RNA compared to 1.93 in wild-type siblings (Paired Student's *t*-test, 0.0371) (Figure 3-16 B). This data suggests that the processing of 28S rRNA and not 18S rRNA is impaired in *nol9*^{sa1022} mutants. Collectively the Northern blot and bioanalyser results demonstrate that the processing of 28S rRNA is impaired in *nol9*^{sa1022} mutants and that the function of Nol9 is conserved from human to zebrafish.

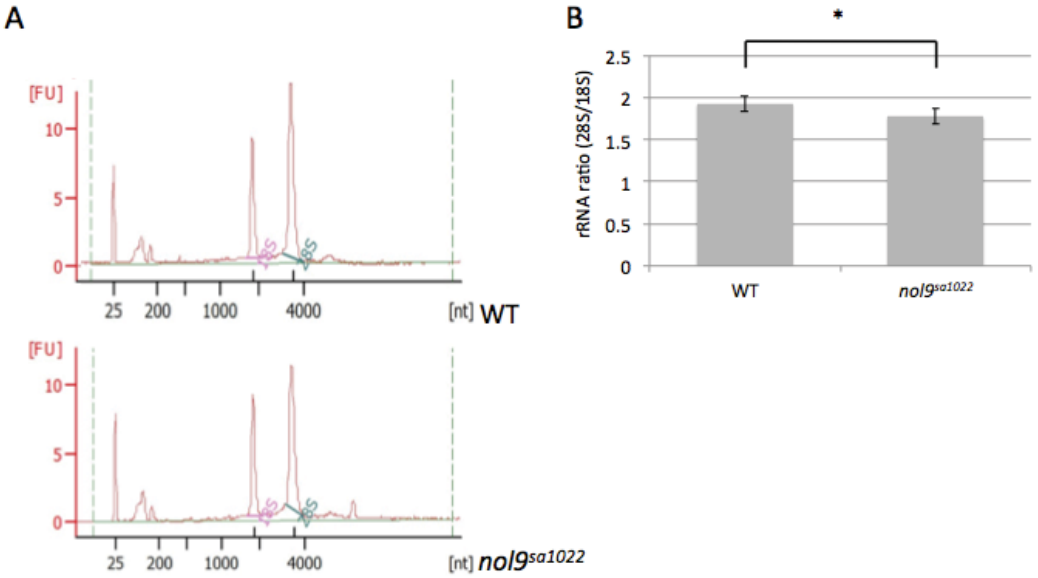

Figure 3-16 The processing of 28S rRNA is impaired in *nol9*^{sa1022} mutants. (A-B) Bioanalyser analysis of total RNA isolated from 5 d.p.f. *nol9*^{sa1022} mutants and wild-type siblings from an incross of *nol9*$^{sa1022/+}$ adults. (A) Representative images of bioanalyser analysis showing a reduction in levels of 28S rRNA but not 18S rRNA in *nol9*^{sa1022} mutants compared to wild-type siblings. (B) The relative rRNA ratio (28S/18S) is statistically significantly smaller in *nol9*^{sa1022} mutants compared to wild-type siblings. Data is representative of four biological replicates as the mean ± SD, Paired Student's *t*-test *p<0.05.

3.2.15 Formation of 60S ribosomal subunit is impaired in *nol9*^{sa1022} mutants

To investigate the effect of the deficiency of Nol9 on ribosome biogenesis, incrosses of *Tg(ins:mCherry)*^{jh2}*;Tg(ptf1a:EGFP)*^{jh1}*;nol9*$^{sa1022/+}$ were phenotyped at 5 d.p.f. based on the size of the *ptf1a*-expressing region. Polysome fractionation was carried out in collaboration with Dr Felix Weis; extracts were prepared from 50 phenotypic and non-phenotypic larvae and the ribosomal subunits were fractionated on sucrose density gradients (Section 2.5.2). The peaks corresponding to the 60S subunits and 80S monosomes in the lysate from *nol9*^{sa1022} mutants are distinctly smaller compared to those in the lysate from wild-type siblings (Figure 3-17). Additionally there are fewer and smaller peaks corresponding to the polysome in the lysate from *nol9*^{sa1022} mutants compared to the lysate from wild-type siblings. In contrast, the peak corresponding to the 40S subunit in the lysate from *nol9*^{sa1022} mutants is larger than that in the lysate from wild-type siblings. This data suggests that the *nol9* mutation affects the formation of the 60S ribosomal subunit and is consistent with the function of Nol9 in processing of 28S rRNA.

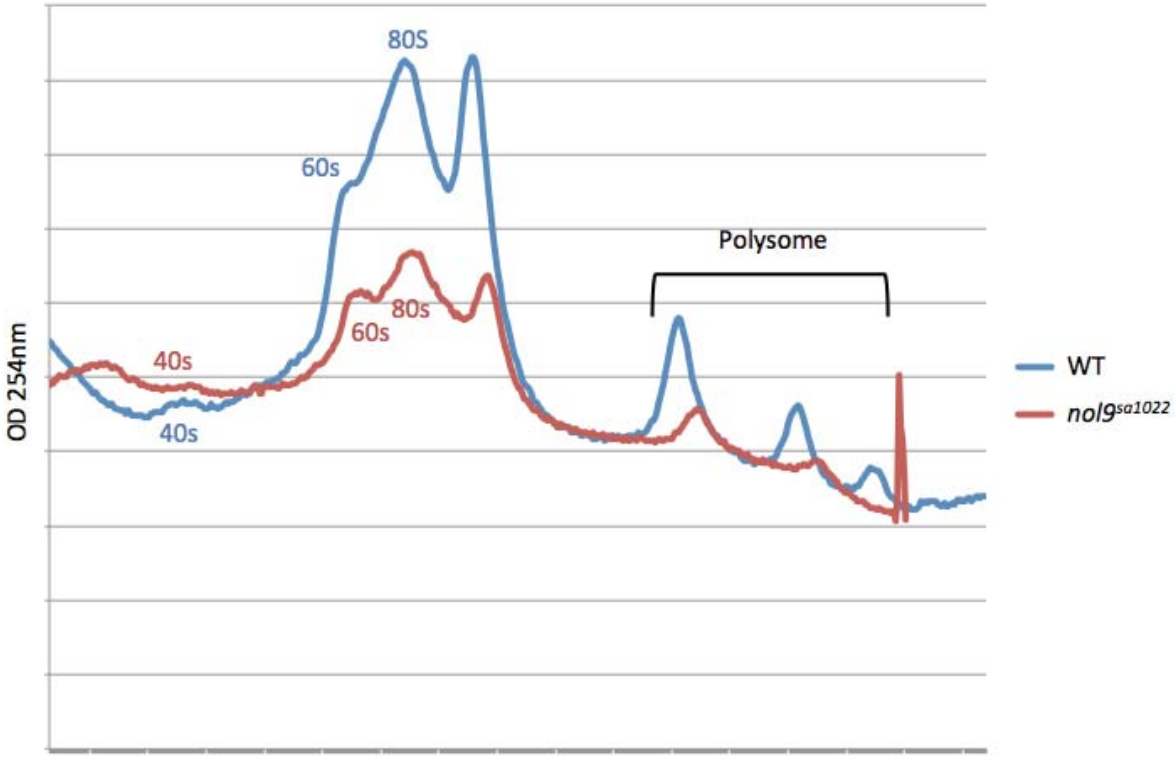

Figure 3-17 60S subunit formation is impaired in *nol9*^{sa1022} mutants. Polysome fractionation analysis performed on *nol9*^{sa1022} mutants and wild-siblings at 5 d.p.f. demonstrating reduced levels of 60S ribosomal subunits, 80S monosomes and polysomes and increased levels of 40S ribosomal subunits in *nol9*^{sa1022} mutants compared to wild-type siblings.

3.3 Discussion

The *nol9*^{sa1022} mutant exhibits a hypoplastic phenotype in digestive organs affecting the pancreas, liver and intestine, and an uninflated swim bladder, whilst the development of other organs appears unaffected. The zebrafish Nol9 protein is indispensable for life as the *nol9*^{sa1022} larvae die before 10 d.p.f.

In humans, the NOL9 protein is required for cleavage at the ITS2 region to generate 5.8S and 28S rRNAs of the large ribosomal subunit (Heindl and Martinez, 2010). The experiments carried out in this study demonstrate that the *nol9*^{sa1022} mutants displayed an accumulation of rRNA intermediates that generate the 5.8S and 28S rRNAs, an increase in the levels of 28S rRNA and reduced levels of 60S ribosomal subunits. These results are consistent with the function of human NOL9 protein. Since the *nol9*^{sa1022} mutation is a nonsense mutation at amino acid 195 in exon 2, it was presumed that this would result in a loss of Nol9 protein. The protein levels in *nol9*^{sa1022} mutants were not tested as commercial antibodies that cross-reacted with zebrafish Nol9 could not be found. The zebrafish Nol9 only shares 34% and 36% identity with human and mouse NOL9.

The development of the pancreas, liver and intestine in *nol9*^{sa1022} mutants proceed normally until 3 d.p.f. but at 4 d.p.f. the digestive organs of *nol9*^{sa1022} mutants are smaller compared to wild-type siblings. The phenotype of *nol9*^{sa1022} is highly reminiscent of other zebrafish mutants of genes encoding rRNA processing proteins namely *nil per os* (*npo*), mutated in gene *RNA binding protein 19* (*rbm19*) (Mayer and Fishman, 2003), *digestive expansion factor* (*def*) (Chen et al., 2005), *titania* (*tti*), mutated in *periodic tryptophan protein 2 homolog* (*pwp2h*) (Boglev et al., 2013) and *nucleolar protein with MIF4G domain 1* (*nom1*) (Qin et al., 2014). Nevertheless, the development of digestive organs in *npo*, *def* and *nom1* were impaired before 3.5 d.p.f. (Chen et al., 2005; Mayer and Fishman, 2003). Using organ-specific markers, we demonstrated that fully differentiated cells were still present in the pancreas and intestine of *nol9*^{sa1022} mutants. This is similar to the *def* and *nom1* mutants where cellular differentiation proceeds in the pancreas, intestine and liver and the *tti* mutant that had fully differentiated intestinal goblet cells (Boglev et al., 2013; Chen et al., 2005). Conversely, cytodifferentiation of the intestine and liver in *npo* mutant were inhibited. It will be interesting to determine whether cellular differentiation proceeds normally in the liver of *nol9*^{sa1022} mutants by doing *in situ hybridisation* with probes against markers of liver

differentiation including *ceruloplasmin* (*cp*) and *fatty acid binding protein 1* (*fabp1*) (Her et al., 2003; Korzh et al., 2001). The *npo*, *def*, *tti* and *nom1* mutants all had additional morphological defects including abnormal jaws, branchial arches and smaller head and eyes (Boglev et al., 2013; Chen et al., 2005; Mayer and Fishman, 2003; Qin et al., 2014). In general, the phenotype of *nol9*^{sa1022} mutants is subtler than the previously described *npo*, *def*, *tti* and *nom1*.

A closer examination of pancreas development in *nol9*^{sa1022} mutants revealed that pancreatic duct formation is impaired. On the other hand, the endocrine cells of the pancreas are formed and fully differentiated and *insulin*-expressing cells of the secondary islets are present in *nol9*^{sa1022} mutants at similar numbers as wild-type siblings. Both pancreatic ducts and secondary islets arise from pancreatic Notch-responsive cells (PNCs) that together with *ptf1a*-expressing cells are derived from the ventral bud (Wang et al., 2011). Hence the pancreatic defect in the *nol9*^{sa1022} mutants is not restricted to a specific cell lineage but instead it is possible that cells that are proliferating at a higher rate are affected by defects in ribosome biogenesis. A more detailed study of secondary islet formation is required where the nascent and other mature endocrine cells (α- and δ-cells) of secondary islets are examined. Also, it will be interesting to investigate the formation of pancreatic ducts and secondary islets in the other rRNA processing mutants, *npo*, *def*, *tti* and *nom1*.

The hypoplastic phenotype of digestive organs of *nol9*^{sa1022} mutants could be due to cell proliferation arrest or increased cell death. The *nol9*^{sa1022} mutants have an increased proportion of cells arrested at the G1 phase implicating defects in cell proliferation. BrdU-labelling revealed that the proliferation rate of the exocrine pancreas of *nol9*^{sa1022} mutants is reduced while the TUNEL assay did not detect an increase in cell death in *nol9*^{sa1022} mutants. These results are in agreement with those of previously reported rRNA processing mutants: the *def* and *tti* mutant larvae showed compromised cell proliferation in digestive organs and in the *nom1* mutant larvae, cell proliferation of the exocrine pancreas was impaired. There was no obvious increase in cell death in all three mutants whilst cell proliferation and cell death were not measured in the *npo* mutant (Boglev et al., 2013; Chen et al., 2005; Mayer and Fishman, 2003; Qin et al., 2014). Future work to help explain the phenotype of the *nol9*^{sa1022} mutants will include studying the cell proliferation of the endocrine pancreas, liver and intestine. Recently, it was discovered that autophagy is induced in intestinal epithelial cells of *tti* mutant to prolong the cell survival and lifespan of the mutant larva (Boglev et al., 2013).

Additionally, red blood cells of zebrafish mutants with deficiency in *ribosomal protein S7* (*rps7*) showed increased autophagy (Heijnen et al., 2014). Studies to determine whether the pancreas, liver and intestine of *nol9*^{sa1022} mutants undergo autophagy will be critical and may corroborate the idea that autophagy is a general response mechanism to ribosomal stress.

The tissue-specific defects resulting from mutations in a gene that is involved in a ubiquitous process could be attributed to the preferential expression of that gene in the tissues affected. The developmental expression pattern of *nol9* follows that of ribosomal biogenesis genes *npo*, *def*, *tti*, *nom1* and multiple *ribosomal protein L* (*rpl*) (Boglev et al., 2013; Chen et al., 2005; Mayer and Fishman, 2003; Provost et al., 2013; Qin et al., 2014). After an initial widespread expression in early embryos, *nol9* and other ribosomal biogenesis genes become increasingly restricted to specific organs including the pancreas, liver and intestine starting from 2 to 3 d.p.f. These organs are amongst the most rapidly proliferating tissues at 3 d.p.f. (de Jong-Curtain et al., 2009). The main hypothesis to explain the tissue specific phenotype of a ubiquitously expressed gene is that wild-type mRNA and/or protein deposited by the heterozygous mother support the development until about 3 d.p.f. (Boglev et al., 2013). Thereafter, rapidly dividing tissues that require large numbers of ribosomes for protein synthesis exhaust the maternally derived wild-type mRNA resulting in a tissue-specific phenotype. This hypothesis however may be an oversimplification since the head of *nol9*^{sa1022} mutants is normal despite *nol9* being highly expressed in the head at 3-4 d.p.f. and the dorsal midbrain and hindbrain proliferating rapidly at 3 d.p.f. (de Jong-Curtain et al., 2009). Therefore, other possibilities that can also contribute to the defects specific to the digestive organs should be considered including Nol9 having digestive organ-specific functions in ribosome biogenesis.

In some ribosomopathies, patients suffer from haematological abnormalities including anaemia (Narla and Ebert, 2010). In 3 d.p.f. and 5 d.p.f. *nol9*^{sa1022} mutants, the blood circulation appeared normal and primitive erythrocytes were present. However, the definitive waves of haematopoiesis that comprise of progenitors of adult cell types in *nol9*^{sa1022} mutants may still be affected. Future work will include analysis of haematopoietic stem cells of the definitive wave by carrying out *in situ hybridisation* using probes against c-*myeloblastosis oncogene* (*c-myb*) and *runt-related transcription factor 1* (*runx1*) (de Jong and Zon, 2005). In addition, the differentiation potential of haematopoietic cells in *nol9*^{sa1022} mutants will be investigated using probes against *recombination activating gene 1* (*rag1*) and *haemoglobin*

alpha embryonic 1 (*hbae1*), markers of differentiated lymphocytes and erythrocytes respectively (de Jong and Zon, 2005). It will be interesting to examine haematopoiesis in adult *nol9*$^{sa1022/+}$ fish since mice heterozygous for the Rpl24 gene, encoding 60S ribosomal protein L24, are characterised by impaired haematopoietic stem cell function due to inefficient protein synthesis (Signer et al., 2014).

The yeast orthologues of *def* and *pwp2h, UTP25* and *PWP2* are both components of the small-subunit (SSU) processome (Bernstein et al., 2007; Charette and Baserga, 2010; Dosil and Bustelo, 2004; Goldfeder and Oliveira, 2010). The SSU processome is a large ribonucleoprotein complex that comprises of the U3 small nucleolar RNA (snoRNA) and at least 43 proteins and is required for biogenesis of the 18S rRNA of the small ribosomal subunit (Bernstein and Baserga, 2004; Dragon et al., 2002). NOM1 and Mrd1p, the yeast orthologue of *npo* are also required for 18S pre-rRNA processing (Alexandrov et al., 2011; Jin et al., 2002). Comparatively, human mutations in *Cirhin*, the homologue of a component of the SSU processome complex, *UTP4* cause liver failure in children, a condition known as North American Indian childhood cirrhosis (NAICC) (Chagnon et al., 2002). *NOL11*, another SSU processome component and an interaction partner for *hUTP4*/Cirhin, is also implicated in the pathogenesis of NAICC (Freed et al., 2012). In addition, exocrine pancreatic dysfunction is one of the clinical features of Shwachman-Diamond syndrome, an inherited bone marrow failure syndrome caused by mutations in *sbds* (Boocock et al., 2003). Although SBDS is a multifunctional protein, its function in the maturation and export of the 60S ribosomal subunit could be instrumental in producing the exocrine pancreatic phenotype (Finch et al., 2011; Menne et al., 2007; Wong et al., 2011b). In general, defective 18S rRNA processing proteins CIRHIN, Def, Pwp2h, Nom1, Npo and large ribosomal subunit biogenesis protein SBDS all result in failure of digestive organs, revealing that digestive organs are particularly sensitive to mutations that impair ribosome production. Therefore it will be unsurprising if digestive organ failure is found to be a regular feature of newly discovered ribosomopathies. Mutations in human *NOL9* have not yet been reported and it is difficult to predict the clinical features of the patients. Nevertheless the loss of function of *nol9* in zebrafish suggests that the human condition could also be characterised by impaired function of digestive organs whereas craniofacial and/or skeletal defects are less likely to be present.

The *nol9*^{sa1022} mutant is the first zebrafish ribosomal biogenesis mutant to be described with morphological defects present only in digestive organs. Studying this mutant further will help elucidate the indispensable role of Nol9 in expansion growth of digestive organs and also facilitate our understanding of the puzzling phenomenon of tissue-specificity resulting from impaired ribosome biogenesis in zebrafish and in ribosomopathies.